


Article

Study on the Application Method of Aquifer Depth Distribution Patterns as Model Input on the Performance of a Physically Based Distributed Hydrologic Model

Jeawhan Shin ¹, Bonwoong Koo ², Jonghwan Jang ², Sunho Choi ² and Changhwan Jang ^{3,*}

¹ Water Resources and Hydrologic Natural Circulation Laboratory, Department of Civil and Environmental Engineering, Daejin University, 1007 Hoguk-ro, Pocheon-si 11159, Republic of Korea; send2u95@naver.com

² Department of Civil and Environmental Engineering, General Graduate School, Daejin University, 1007 Hoguk-ro, Pocheon-si 11159, Republic of Korea; goobw@naver.com (B.K.); hjj0128@naver.com (J.J.); ing0096@hanmail.net (S.C.)

³ Department of Smart Construction and Environmental Engineering, Daejin University, 1007 Hoguk-ro, Pocheon-si 11159, Republic of Korea

* Correspondence: cjang@daejin.ac.kr; Tel.: +82-031-539-1394

Abstract: Groundwater discharge is critical for maintaining river flow during dry seasons, especially in lowland areas. Despite its significance, groundwater resources have often been overlooked highlighting the need for comprehensive studies amidst growing pressure to develop new water resources. This study focuses on the Soyang River Basin, South Korea, including its ungauged northern regions, the nearby DMZ (Demilitarized Zone), using the physically based Gridded Surface Subsurface Hydrologic Analysis (GSSHA) model. A three-year simulation was conducted to examine variable aquifer depth distribution patterns by assuming an inverse relationship between surface elevation and aquifer bottom depth. Three case studies (i.e., equal distribution, linear regression, and logarithmic regression) were evaluated and compared. The method to identify optimal aquifer depth distributions to enhance groundwater simulation accuracy in regions with significant topographical variation was incorporated. Groundwater levels at six monitoring sites showed that altitude-based variable aquifer depths outperformed the equal distribution case. The results showed strong agreement between simulated and observed values, particularly in the linear regression case with an R-squared statistic of 0.858 and Nash–Sutcliffe Efficiency index of 0.789, indicating that linear regression-based aquifer depth estimation can significantly improve long-term runoff modeling and groundwater simulation accuracy. The logarithmic regression case had the lowest relative peak error in peak flow. These findings highlight the importance of adjusting aquifer depth distributions in physically based hydrologic models to better reflect real-world conditions. Overall, this study contributes to advance groundwater modeling by integrating variable aquifer depth distributions into a physically based hydrologic model for large scale watersheds.

Keywords: physically based model; distributed model; groundwater; aquifer depth; hydrological modeling; surface-subsurface



Citation: Shin, J.; Koo, B.; Jang, J.; Choi, S.; Jang, C. Study on the Application Method of Aquifer Depth Distribution Patterns as Model Input on the Performance of a Physically Based Distributed Hydrologic Model. *Water* **2024**, *16*, 3518. <https://doi.org/10.3390/w16233518>

Academic Editors: Chin H Wu and Andrzej Witkowski

Received: 13 September 2024

Revised: 1 December 2024

Accepted: 3 December 2024

Published: 6 December 2024



Copyright: © 2024 by the authors. Licensee MDPI, Basel, Switzerland. This article is an open access article distributed under the terms and conditions of the Creative Commons Attribution (CC BY) license (<https://creativecommons.org/licenses/by/4.0/>).

1. Introduction

In the past century, the world has witnessed increased damage due to climate change, including droughts, heavy downpours, increased intensity of cyclones, and sea level rise. Experts in these fields predict that many countries will face severe water shortages due to the rapid increase in water usage driven by population growth and uneven distribution of water resources. According to a survey by Population Action International (PAI), South Korea is classified as a water-scarce country, along with Kenya, Morocco, and South Africa [1]. Additionally, forecasting of water availability has gained increased attention in recent decades, especially due to growing human pressure and climate change, affecting groundwater resources towards a perceivable depletion [2]. Groundwater resources

are, therefore, of paramount importance [3,4]. Groundwater discharge serves as a crucial source of streamflow during dry periods in lowland rivers. However, despite this importance, insufficient attention has been given to groundwater resources. With the urgent need for developing new water sources, more research on groundwater and aquifers is warranted [5].

The watershed circulation model employed in this study is a hydrological tool capable of replicating the process from rainfall to runoff. Currently, streamflow measurements are primarily conducted in flood forecasting areas, upstream of dams, major rivers, and key points within watersheds, making it difficult to estimate streamflow in ungauged watersheds, medium and small rivers, and sub-watersheds [6]. Initially, models were only able to simulate runoff processes at a basic level. However, with improvements in technology, the number of parameters applied in watershed models has increased, enhancing both theoretical reliability and complexity [7]. Among lumped and distributed models, lumped models rely on empirical formulas derived from observational data, whereas distributed models physically calculate runoff processes using spatial and temporal parameters of each grid, offering greater reliability [8]. Physically based hydrological models are highly applicable in ungauged watersheds and can provide reasonable predictions without extensive calibration efforts [9]. Physically based distributed models interpret hydrological phenomena based on the topographic parameters of a watershed and simulate streamflow at all points within the watershed using optimized parameters for specific locations [10]. Furthermore, given the current situation where flood damage in downstream South Korea is exacerbated by the water resource management practices in upstream North Korea, distributed models, which are advantageous for application in ungauged watersheds, can be effectively utilized [11].

The lithology of aquifers is another important factor influencing the response of groundwater levels to precipitation [12]. The influence of aquifers is closely related to groundwater levels, which ultimately serve as a crucial factor in the long-term runoff of rivers, including both dry and wet seasons. Groundwater levels in aquifers significantly influence long-term river's flows during dry and wet seasons. Among these, physically based models simulate groundwater recharge and aquifer flow using fundamental physical laws [12]. However, in South Korea, where lumped models relying on empirical formulas are predominant, research on parameter optimization applicable to distributed models remains insufficient. Pinder et al. (1968) developed a digital computer program to model unsteady-state fluid flow in confined aquifers using linear parabolic partial differential equations and an implicit finite-difference technique [13]. While this study provides insights into fluid flow using numerical simulations, it is limited by its focus on a confined aquifer with a restricted spatial scope. Golmohammadi et al. [14] conducted a hydrological simulation for the 52.6 km² Canagagigue watershed to evaluate three widely used distributed hydrological models: the Agricultural Policy/Environmental Extender (APEX), the European Hydrological System Model MIKE SHE, and the Soil and Water Assessment Tool (SWAT). These distributed models incorporate a physically based approach, though some empirical calculations are also included. While these models are widely used in distributed hydrological modeling, they do not represent vertical stratification within the aquifer structure, nor do they consider aquifer depth as spatially variable. Additionally, Chung et al. [15] connected the SWAT model with the Transient Water Table Fluctuation Method (TWTFM) to estimate recharge in the river basins of Jeju Island, South Korea. Similarly, Ware et al. [16] applied the SWAT-MODFLOW and TWTFM methods to evaluate groundwater recharge in the Anyang watershed (137 km²) in South Korea. These studies [15,16] are significant as they represent the first application of coupled models for assessing groundwater recharge. These studies showed that groundwater does not remain confined to a single, small watershed. Instead, it flows across larger areas with indistinct boundaries. While models like MODFLOW excel in precise analyses over smaller regions, they face limitations in capturing the long-term behavior of groundwater in extensive watersheds.

Although many hydrological models today utilize physically based distributed modeling approaches, it remains practically impossible to accurately assess how aquifer depth is distributed across large-scale watersheds. As a result, there is no standardized method for applying the aquifer depth layer in hydrological models, and it is common to assume that the aquifer exists at a uniform depth from the surface. However, applying a uniform aquifer depth without proper justification contradicts the principles of physically based models. Therefore, when performing physically based distributed hydrological modeling at the watershed scale, aquifer depth should be determined based on solid physical evidence.

This study contributes to the groundwater modeling literature by presenting a novel method for incorporating spatially variable aquifer depth into physically based distributed models at a watershed scale. Focusing on the large-scale Soyang River Basin in South Korea, covering an area of 2789 km², we propose two methods for estimating aquifer depth on a grid-cell basis, based on an assumed correlation between surface elevation and aquifer depth. By applying these calculated aquifer depth layers within a physically based distributed hydrologic model, we enable reliable simulations of groundwater recharge and surface runoff across diverse terrain conditions. The applicability of this method has been demonstrated for large-scale watershed modeling, such as in the Soyang River Basin, enhancing the use of physically based distributed hydrologic models under various watershed conditions. Furthermore, this approach, grounded in solid physical principles, offers a more realistic alternative to conventional methods of applying aquifer depth in watershed modeling, providing reliable predictions essential for comprehensive, long-term water resource planning. To our knowledge, there have been no reported cases of using a physically based distributed model to evaluate groundwater recharge and surface runoff in such a large watershed, nor have there been instances where this assumption regarding aquifer depth has been applied in a hydrologic model. This will be the first instance presented in our research.

2. Methodology

This study applied the Gridded Surface Hydrologic Analysis (GSSHA) model to conduct a detailed hydrological analysis in the Soyang River Basin, incorporating both surface water and groundwater processes. The model's capability to integrate surface water runoff, groundwater infiltration and exfiltration, and changes in groundwater levels allows for a comprehensive simulation framework. Physically based hydrological models offer a significant advantage in ensuring parameter reliability, as they are based on physical calculations rather than empirical formulas. This enhances the accuracy and applicability of simulations, particularly in ungauged watersheds.

Currently, most hydrological models assume a uniform aquifer depth below the surface for large watershed-scale groundwater simulations, which oversimplifies the complexity of real-world conditions. However, in reality, aquifer depth is spatially variable. This study addresses this limitation by applying a more realistic aquifer depth distribution, assuming a nonlinear inverse relationship between surface elevation and aquifer depth. This approach better reflects the natural variability of aquifer thickness across different elevations, providing a more accurate representation of groundwater processes.

The research methodology consists of the following steps:

1. **Baseline Model Setup:** The baseline model for comparing aquifer depth distribution methods was constructed with a focus on streamflow. We confirmed that the model's surface runoff and infiltration stages were functioning correctly. During this phase, validation and calibration of parameters excluding groundwater simulations were performed.
2. **Analysis of Elevation and Aquifer Depth Regression Relationship:** Referencing national groundwater observation network data and groundwater measurement reports for the study area, we analyzed the regression relationship between the surface elevation patterns and aquifer depths in the target region. It is essential to recognize that the limited number of groundwater depth measurement points relative to surface

- elevation data introduces some uncertainty in this study. Therefore, we analyzed the regression relationship using the currently available data.
3. **Aquifer Depth Configuration:** The first method employed is a commonly used approach in large-scale watershed simulations, which assumes a uniform aquifer depth at a specified distance from the surface. The second method involves non-uniform aquifer depth settings, utilizing two models based on previously analyzed surface elevation and aquifer depth data through logarithmic and linear regression equations. This non-uniform depth distribution method considers spatial variability and proposes implementing a nonlinear inverse relationship between surface elevation and aquifer depth. These methods allow for a dynamic setting of aquifer depth across diverse terrain and elevations within the watershed, facilitating more realistic simulations.
 4. **Simulation Calibration:** Using both the uniform and non-uniform aquifer depth models, we simulated the hydrological processes that include groundwater. The simulation period was divided into calibration and validation phases, ensuring that various parameters, such as initial groundwater levels and soil moisture, stabilized during the calibration phase while replicating the hydrological processes.
 5. **Simulation Validation:** The validation process compared the simulated results of streamflow and groundwater levels with observed data obtained from national observation points. This study proposes a new method for hydrological modeling that includes groundwater simulation and verifies its applicability, aiming to better reflect the physical processes involved. The research flow chart is illustrated in Figure 1, the research flowchart.

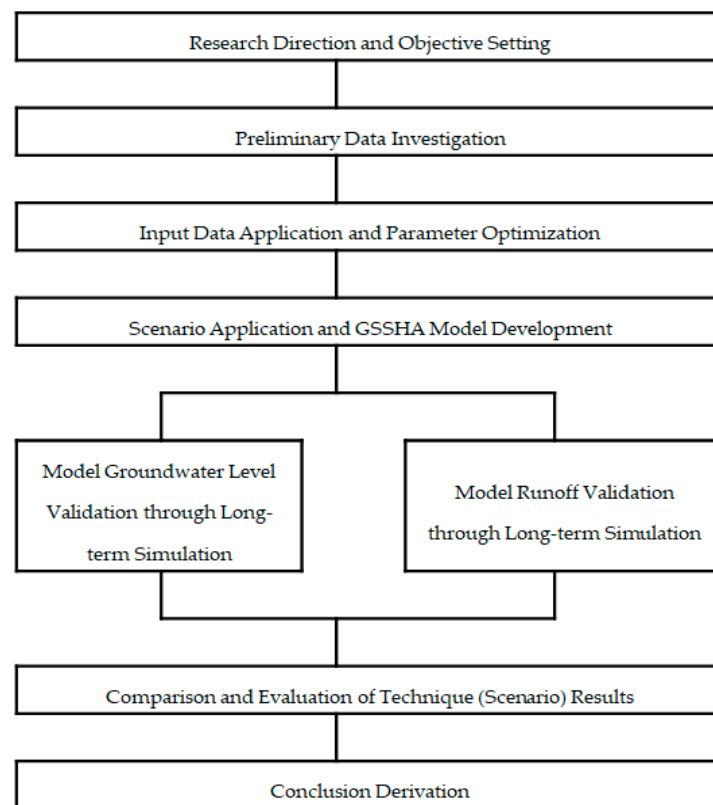


Figure 1. Research flowchart.

This approach seeks to improve the reliability of groundwater simulations by applying more physically grounded methods of estimating aquifer depth. By comparing results from both the uniform and non-uniform aquifer depth models, this research aims to provide insights into how aquifer thickness distribution affects hydrological modeling accuracy,

thus contributing to better water resource management, particularly in the context of drought preparedness.

2.1. Study Area

2.1.1. Overview and Location

The Soyang River Basin was selected as the study area to analyze the spatial-distribution technique of aquifer depth parameters through groundwater simulation. According to the study by Shin [17] on the impacts of climate change on the Bukhan River Basin, including the Soyang River and areas in North Korea, the Soyang River Basin is projected to face the highest drought risk as climate change intensifies. Additionally, although the area includes ungauged regions along the border with North Korea, the downstream regions in the southern basin contain numerous water and groundwater observation stations, making it a suitable study area for this research. The Soyang River Basin spans 164.9 km in length and covers an area of 2789 km², comprising the national river, the Soyang River, and 31 local rivers. The Soyang River Dam, located within the basin, is the largest multipurpose dam in South Korea, capable of storing 2.9 billion m³ of water, serving both flood control and water supply functions during drought periods. Additionally, the Inbukcheon tributary of the Soyang River, which borders the northern Demilitarized Zone (DMZ), includes 155.15 km², or 16.68% of its watershed area, located north of the DMZ, an ungauged zone. The geographic location of the study area is shown in Figure 2 [18,19].

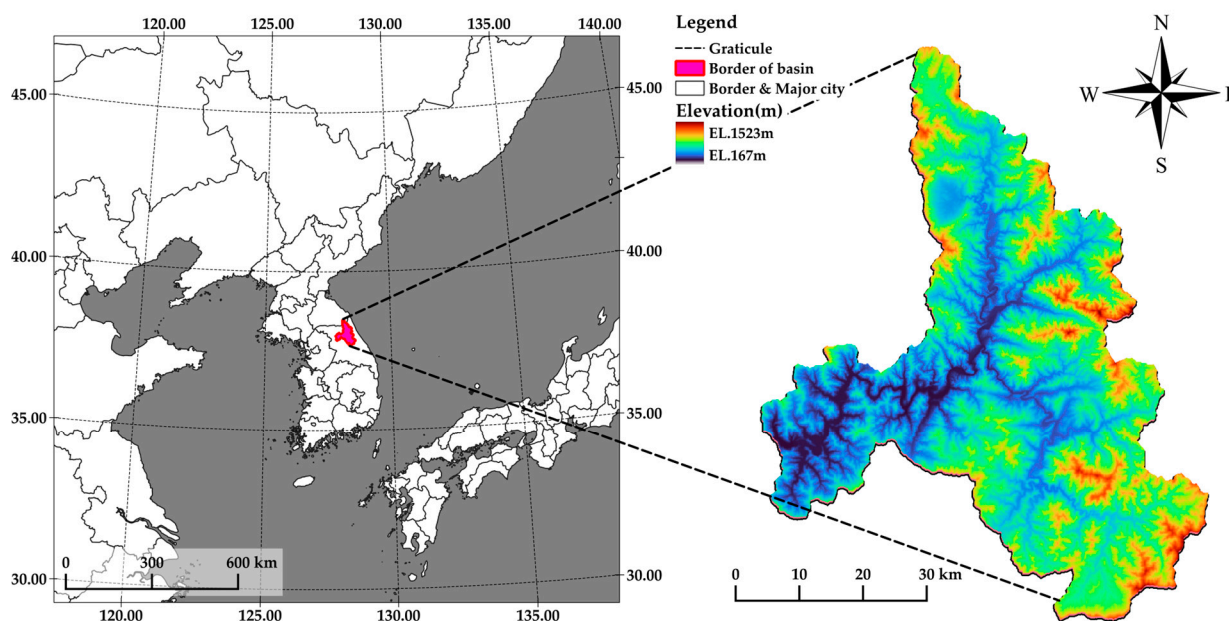


Figure 2. Location of the study area.

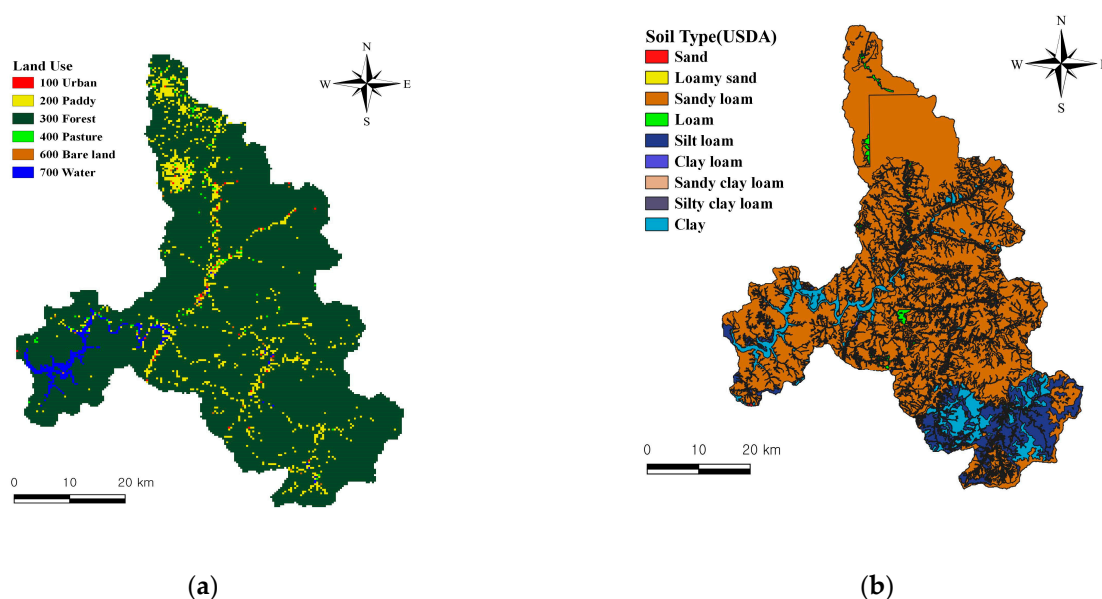
2.1.2. Land Cover and Soil Characteristics

The land cover data used in this study were prepared according to the Land Cover Mapping Guidelines (KME, 2018) provided by the Ministry of Environment of South Korea. For the area south of the DMZ, 2016 land cover data from the Ministry of Environment were used [20]. For the area north of the DMZ, land cover data from the 1990s, collected during past surveys, were utilized. These two data sets were merged, and changes in land cover were applied using satellite imagery. The area for each land cover type in the Soyang River Basin is shown in Table 1.

Table 1. Area by land cover type.

Land Cover Classification	Area (km ²)	Area (%)
100 (Urban)	5.70	0.21
200 (Paddy)	170.38	6.38
300 (Forest)	2430.58	91.01
400 (Pasture)	14.25	0.54
500 (Wet land)	0	0
600 (Bare land)	5.83	0.21
700 (Water)	43.93	1.65

The soil properties data used in this study were sourced from different regions. For the area south of the DMZ, the detailed soil map provided by the National Institute of Agricultural Sciences (NIAS) of Korea was used. This map is classified into 68 soil series codes. For the area north of the DMZ, data collected for military purposes in the past were utilized, consisting of soil properties classified by the United States Army Corps of Engineers (USACE). These two data sets were reclassified into unified soil properties based on the soil-classification criteria proposed by Heo and Jung (1987) [21]. This reclassification was done according to the Soil Conservation Service (SCS) hydrological soil group definitions, considering factors such as soil texture, permeability, soil depth, infiltration rate, organic matter content, and soil expansion capacity. The land cover and soil maps of the Soyang River Basin used in this study are shown in Figure 3.

**Figure 3.** Properties of the Soyang River Basin. (a) Land cover type; (b) soil type data.

2.2. GSSHA Distributed Model

The Gridded Surface Subsurface Hydrologic Analysis (GSSHA) model was developed by the US Army Corps of Engineers Engineering Research and Development Center (USACE ERDC). GSSHA evolved from the CAS2D and is a distributed hydrologic and water quality model based on the physical calculation process of parameters.

GSSHA divides a watershed into equal finite-difference grid cells. Calculations for each time step after rainfall are performed at the level of individual grid cell, and the responses from each grid cell are integrated to generate the overall watershed response. The main components of the model include algorithms for rainfall distribution, snow accumulation and melt, rainfall interception, infiltration, evapotranspiration and transmission, surface water retention, surface runoff routing, channel flow routing, unsaturated zone modeling,

saturated groundwater flow, land sediment erosion, transport and deposition, and sediment routing. The applied model components and framework are shown in Figure 4.

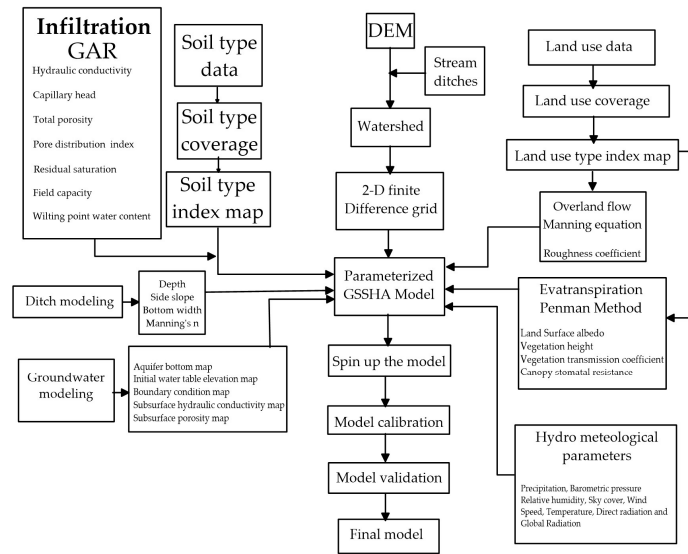


Figure 4. Model components and framework.

While most hydrologic models focus on Hortonian runoff analysis, GSSHA is capable of analyzing both Hortonian and non-Hortonian runoff, making it applicable to a wide range of climates and watersheds. Additionally, the model includes modules for unsaturated flow and saturated groundwater aquifer analysis, and it has significantly improved in stability and efficiency compared to its predecessor, CAS2D [22]. Figure 5 illustrates the simulation flowchart of the GSSHA model.

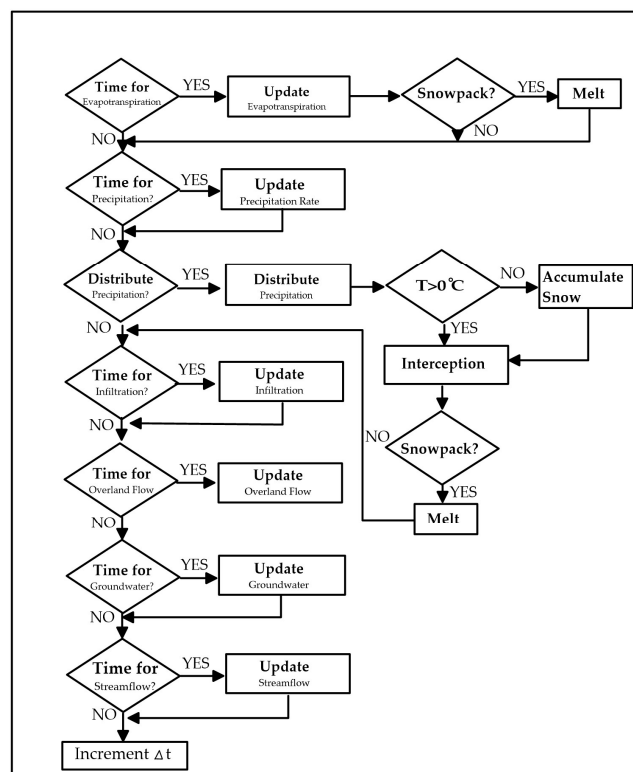


Figure 5. Simulation flow chart of GSSHA.

2.3. Hydrological Processes and Model Configuration

2.3.1. Surface Runoff Modeling

In this study, the grid size forming the basis of the distributed model was determined to be 990 m × 990 m through several trial runs. The Soyang River Basin comprises a total of 2730 grids. The threshold for flow accumulation was set at 2.89 km², and the final stream network was generated by aligning the calculated flow accumulation results with the specified grid size.

Surface runoff uses methods similar to one-dimensional channel routing, but the calculations are performed considering two dimensions. The flow per unit width between grid cells is expressed as discharge p_{ij} and q_{ij} , with a dimension of m³/s, and is calculated with depth d_{ij} in the i and j cells. The roughness coefficient at the n -th time step is denoted as n_{ij} , and Manning's equation is used to spatially vary the roughness coefficient. The total discharge head in the x and y directions is expressed as shown in Equations (1) and (2).

$$p_{ij}^n = \frac{1}{n_{Mij}} \left(d_{ij}^n \right)^{\frac{5}{3}} \left(S_{fx}^n \right)^{\frac{1}{2}} \quad (1)$$

$$q_{ij}^n = \frac{1}{n_{Mij}} \left(d_{ij}^n \right)^{\frac{5}{3}} \left(S_{fy}^n \right)^{\frac{1}{2}} \quad (2)$$

The outflow of each cell is calculated based on the flow at the $(n + 1)$ -th time step [23].

$$d_{ij}^{n+1} = d_{ij}^n + \frac{\Delta t}{\Delta x} \left(P_{i-1,j}^n + q_{i,j-1}^n - P_{ij}^n - q_{ij}^n \right) \quad (3)$$

In the surface runoff process, surface roughness coefficients based on land cover can be input, and the parameters can be entered in a spatial distribution format. The land cover map applied to the GSSHA model was constructed using WMS and QGIS. The range of surface roughness coefficients for various land covers was referenced from the values presented in the studies by Huggins et al. (1966) [24], Engman (1986) [25], Park et al. (2008) [26], and Hjelmfelt (1986) [27], and the optimal roughness coefficients were applied through model calibration. The average roughness coefficient values determined by Hjelmfelt (1986) [27] were found to be closest to actual measurements and had the smallest deviations, and thus they were applied to the eight major classification systems categorized by the Ministry of Environment of South Korea. The grid-based elevation and river network created by the GSSHA model, along with the grid-based land cover classification, are shown in Figure 6, and the range of roughness coefficients by land cover applied in this study is presented in Table 2.

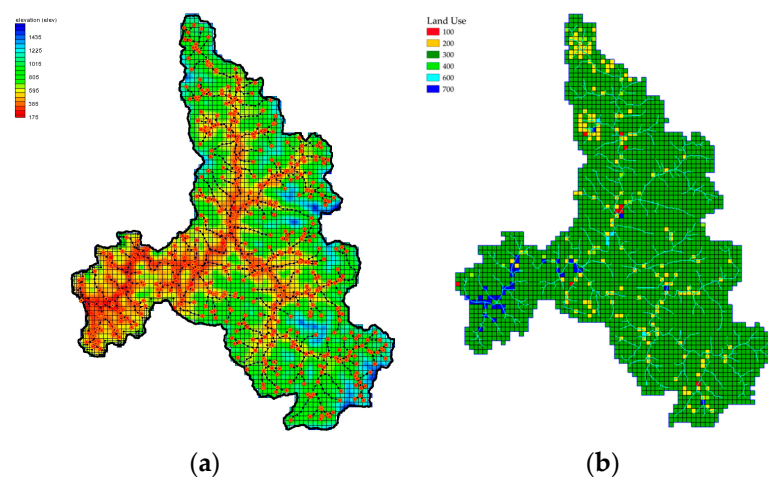


Figure 6. GSSHA terrain and land cover layer. (a) Terrain layer (elevation, stream); (b) grid-based land cover layer.

Table 2. Range of roughness coefficient.

Classification Code	Range (n)	Adoption (n)
100 (Urban)	0.0137~0.1	0.043
200 (Paddy)	0.02~0.09	0.05
300 (Forest)	0.1~0.4	0.231
400 (Pasture)	0.035~0.15	0.112
600 (Bare land)	0.02~0.07	0.04
700 (Water)	0.015~0.02	0.015

2.3.2. Infiltration Modeling

The Green–Ampt Multi-Layer infiltration model was utilized for the infiltration analysis. The Multi-Layer function allows for the input of infiltration parameters for three different layers within each soil series. These parameters include hydraulic conductivity (cm/h), pore distribution index (cm/cm), capillary head (cm), field capacity (m³/m³), wilting point (m³/m³), total porosity (cm³/cm³), residual saturation (m³/m³), initial soil moisture (%), and soil depth (cm). The Green–Ampt model is theoretically based on Darcy’s Law.

$$f = K \left(\frac{F + \Delta\theta\psi}{F} \right) \tag{4}$$

By integrating with respect to F under the condition F = 0 at t = 0, the equation for cumulative infiltration is obtained as

$$F(t) = Kt + \Delta\theta\psi \ln \left(1 + \frac{F(t)}{\Delta\theta\psi} \right) \tag{5}$$

In the equation, K is the hydraulic conductivity, t is time, ψ is the capillary head, and Δθ is the soil moisture deficit.

The mechanism of the Green–Ampt infiltration model is shown in Figure 7 [17]. The ranges of these parameters, based on Rawls et al. (1983) [28], were applied to estimate the infiltration parameters according to soil layer depth. The Green–Ampt parameters for each soil layer were applied to the 43 soil series in the Soyang River Basin. The application of the 43 South Korea Soil Series Codes in the GSSHA model is shown in Figure 8, and the soil properties by soil layer depth for each soil series are presented in Table 3. Additionally, the infiltration parameters by soil properties are provided in Table 4. The soil parameters for the Green–Ampt model were derived from the geometric mean of a large number of soil samples. However, these parameters have a high degree of variability, leading to uncertainty between textural classifications and soil textures. The adjustment and optimization of Green–Ampt infiltration coefficients and related parameters were referenced from Triadis et al. (2012) [29].

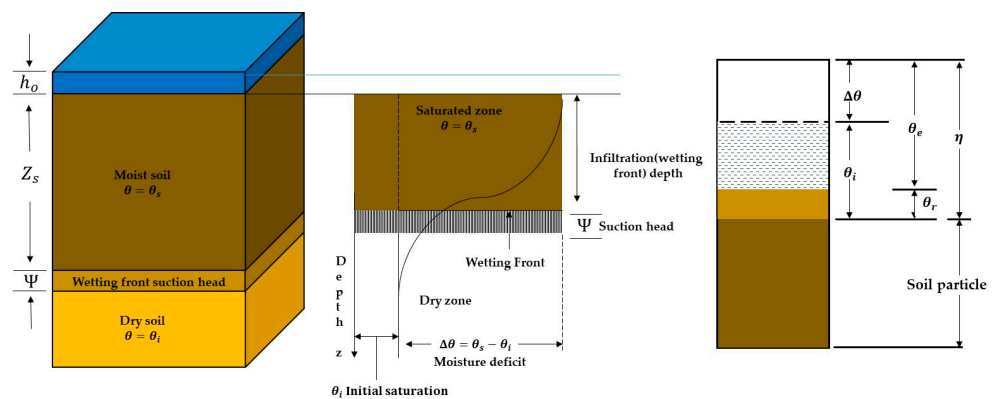


Figure 7. Green–Ampt infiltration model (Shin, 2022) [17].

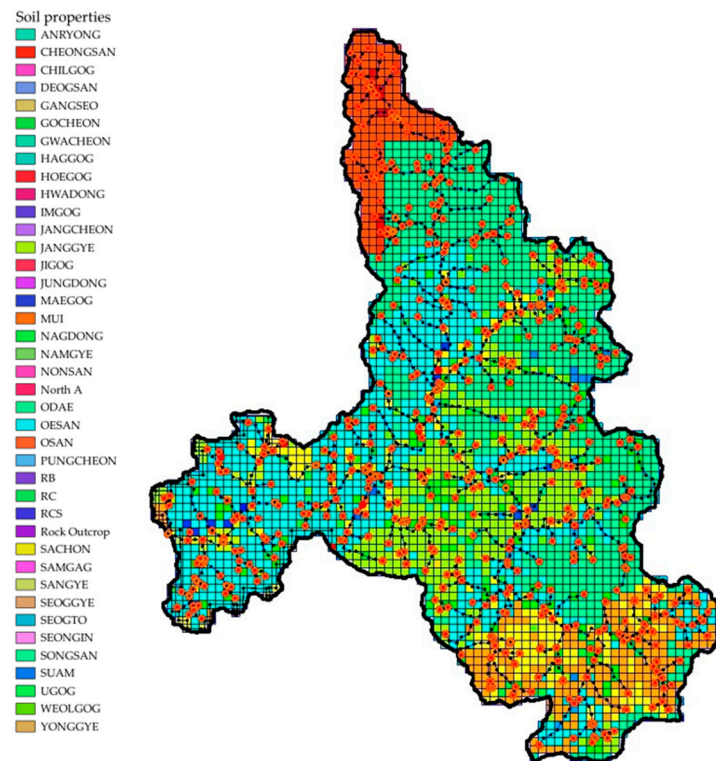


Figure 8. GSSSHA soil properties layer.

Table 3. Soil property input data by soil layer depth based on Korean soil series codes.

South Korea Soil Series Codes	Soil Layer Depth (cm) and Soil Properties		
	Layer 1	Layer 2	Layer 3
IMGOG	Clay loam (16)	Loam (45)	Clay loam (89)
OESAN	Silt loam (15)	Silt loam (48)	Loam (35)
GOCHEON	Loam (18)	Loam (43)	Sandy loam (89)
YONGGYE	Loam (21)	Loam (73)	Clay loam (72)
NAGDONG	Loamy sand (23)	Sandy loam (72)	Sandy loam (85)
ANRYONG	Silt loam (22)	Silty clay loam (33)	Silty clay loam (65)
DEOGSAN	Sandy loam (17)	Clay (90)	Clay (90)
CHILGOG	Loam (15)	Clay loam (78)	Clay loam (68)
CHEONGSAN	Silt loam (10)	Silty clay loam (62)	Clay (90)
GANGSEO	Sandy loam (20)	Loam (32)	Loam (98)
WEOLGOG	Sandy loam (26)	Loam (44)	Loamy sand (40)
ODAE	Sandy loam (18)	Sandy loam (32)	Clay (90)
SACHON	Loam (22)	Loam (62)	Loamy sand (66)
SONGSAN	Loam (20)	Sandy loam (62)	Sandy loam (78)
HDB	Loam (22)	Sandy loam (63)	Sandy loam (75)
JANGCHEON	Loamy sand (8)	Sand (57)	Loamy sand (55)
NONSAN	Silt loam (13)	Silty clay loam (62)	Sandy clay loam (95)
HAGGOG	Sandy loam (20)	Loamy sand (35)	Sandy loam (95)
UGOG	Silt loam (14)	Silt loam (36)	Silty clay loam (145)
PUNGCHAEON	Sandy loam (14)	Loam (38)	Loam (73)
North A		Clay loam (158)	
North C		Clay (158)	
North D		Silty clay loam (158)	
North F		Sandy loam (158)	
MAEGOG		Sandy loam (149)	
JUNGDOONG		Sandy loam (160)	
NAMGYE		Sandy loam (150)	
Water		Clay (160)	
SAMGAG		Sandy loam (180)	
SEONGIN		Loam (150)	
SUAM		Sandy loam (120)	

Table 3. Cont.

South Korea Soil Series Codes	Soil Layer Depth (cm) and Soil Properties		
	Layer 1	Layer 2	Layer 3
RCS		Sandy loam (137)	
MUI		Sandy loam (160)	
SEOGTO		Silty clay loam (160)	
RB		Sandy loam (126)	
RC		Sandy loam (145)	
JANGGYE		Loam (150)	
HOEGOG		Sandy loam (160)	
JIGOG		Sandy loam (160)	
GWACHEON		Loam (150)	
Rock Outcrop		Clay (198)	
OSAN		Silt loam (180)	
SEOGGYE		Sandy loam (160)	

Table 4. Infiltration parameters by soil properties (Rawls et al. 1983) [28].

Parameters	Hydraulic Conductivity (cm/h)	Pore Distribution Index (cm/cm)	Capillary Head (cm)	Total Porosity (cm ³ /cm ³)	Field Capacity (m ³ /m ³)	Wilting Point (m ³ /m ³)	Residual Saturation (m ³ /m ³)
Sand	11.78	0.298~1.090	0.97~25.36	0.374~0.5	0.018~0.164	0.007~0.059	0.001~0.039
Loamy sand	2.99	0.234~0.872	1.35~27.94	0.368~0.506	0.06~0.19	0.019~0.091	0.003~0.067
Sandy loam	1.09	0.140~0.616	2.67~45.47	0.351~0.555	0.126~0.288	0.031~0.159	0.000~0.106
Loam	0.66	0.086~0.418	1.33~59.38	0.375~0.551	0.195~0.345	0.069~0.165	0.000~0.074
Silt loam	0.34	0.105~0.363	2.92~95.39	0.420~0.582	0.258~0.402	0.078~0.188	0.000~0.058
Sandy clay loam	0.15	0.079~0.559	4.42~108	0.332~0.464	0.186~0.324	0.085~0.211	0.000~0.137
Clay loam	0.1	0.070~0.414	4.79~91.1	0.409~0.519	0.250~0.386	0.115~0.279	0.000~0.174
Silty clay loam	0.1	0.039~0.315	5.67~131.5	0.418~0.524	0.304~0.428	0.138~0.278	0.000~0.118
Sandy clay	0.06	0.048~0.398	4.08~140.2	0.37~0.49	0.245~0.433	0.162~0.316	0.000~0.205
Silty clay	0.05	0.040~0.260	6.13~139.4	0.425~0.533	0.332~0.442	0.193~0.307	0.000~0.136
Clay	0.03	0.037~0.293	6.39~156.5	0.427~0.523	0.326~0.466	0.000~0.136	0.000~0.195

The precision soil map of South Korea was merged with the soil map of USACE to classify soil properties uniformly based on drainage grades. The soil types were then classified using the USDA triangular classification method according to the physical properties of each soil type, including particle size, soil drainage, and permeability.

2.3.3. Stream Flood Routing

The elevations of the model's grid cells are generated from the Digital Elevation Model (DEM), and the extracted stream slopes can cause issues such as reverse slopes within the channel due to terrain distortions. To address these reverse slopes that could cause issues in the simulation, the channel smoothing function within GSSHA was employed. This function, based on an algorithm developed by Ogden (1994) [30], corrects the tendency of DEM to exaggerate concave areas around rivers. For inputting river parameters within the Soyang River Basin, roughness coefficient (n), depth (m), and width (m) were referenced from Basic River Plans for the Upper and Lower Soyang River and the Inbukcheon Area (Ministry of Land, Transport and Maritime Affairs, 2012) [31,32]. The width was verified and adjusted by using Google Earth Pro to closely match the actual river width. Furthermore, when rivers or streams are obstructed by dams or gates, the backwater effect, which causes changes in water flow and upstream water level, was considered.

Rainfall occurring in individual grid cells undergoes interception and infiltration processes, gradually saturating the soil. Once the soil becomes saturated and surface flow begins, the flow proceeds in the two-dimensional x - and y -directions based on the elevation of the grid cell. During this process, the flow velocity is influenced by the surface roughness coefficient. As this surface flow continues and reaches the stream area, stream flow analysis begins. When surface flow meets the channel, the flow velocity increases as if it were moving through a pipe, altering the flow characteristics. In natural rivers, unsteady flow can exhibit diffusion effects due to attenuation during the propagation of flood waves, a phenomenon referred to as a diffusion wave. The flow of a diffusion wave is steady

nonuniform flow, which accounts for the attenuation of the flood wave. To account for these attenuation effects, the diffusive wave was applied in the analysis of stream flow.

The continuity equation of the conservative two-dimensional shallow water equation is provided by Equation (6) as follows:

$$\frac{\partial h}{\partial t} + \frac{\partial hu}{\partial x} + \frac{\partial hv}{\partial y} = 0 \tag{6}$$

By substituting the continuity equation into the momentum equation and dividing both sides by h, the non-conservative equations in the x-direction and y-direction can be expressed as shown in Equations (7) and (8).

$$\frac{\partial u}{\partial t} + u \frac{\partial u}{\partial x} + v \frac{\partial u}{\partial y} + g \frac{\partial h}{\partial x} = g(S_{0x} - S_{fx}) \tag{7}$$

$$\frac{\partial v}{\partial t} + u \frac{\partial v}{\partial x} + v \frac{\partial v}{\partial y} + g \frac{\partial h}{\partial y} = g(S_{0y} - S_{fy}) \tag{8}$$

Rearranging the above Equations (7) and (8) with respect to the water surface slope yields the following Equation (9).

$$S_f = S_0 - \frac{\partial h}{\partial x} - \frac{u}{g} \frac{\partial u}{\partial x} - \frac{1}{g} \frac{\partial u}{\partial t} \tag{9}$$

Additionally, in the momentum equation for the x-direction, the terms containing v can be neglected because $v \ll u$, and in the momentum equation for the y-direction, the terms containing u can be neglected because $u \ll v$. Therefore, the momentum equations in the x- and y-directions, considering the diffusive wave approximation, can be expressed as shown in Equations (10) and (11).

$$S_{fx} = S_{0x} - \frac{\partial h}{\partial x} \tag{10}$$

$$S_{fy} = S_{0y} - \frac{\partial h}{\partial y} \tag{11}$$

In the equation, h is the water depth, u is the velocity in the x-direction, v is the velocity in the y-direction, g is the gravitational acceleration, S_{0x} and S_{0y} are the bed slopes in the horizontal directions, and S_{fx} and S_{fy} are the water surface slopes in the respective horizontal directions

Using Equations (9)–(11), the flow in the x- and y-directions at each grid cell is calculated to perform computations for a single time interval, and the flow rates p and q between the grids are determined. By taking the difference to estimate the bottom slope and water surface slope in Equations (10) and (11), it can be expressed as Equations (12)–(15).

$$S_{0x} = \frac{z_{i,j} - z_{i+1,j}}{\Delta s} \tag{12}$$

$$S_{0y} = \frac{z_{i,j} - z_{i,j+1}}{\Delta s} \tag{13}$$

$$S_{fx} = \frac{z_{i,j} - z_{i+1,j} + h_{i,j} - h_{i+1,j}}{\Delta s} \tag{14}$$

$$S_{fy} = \frac{z_{i,j} - z_{i,j+1} + h_{i,j} - h_{i,j+1}}{\Delta s} \tag{15}$$

z_{ij} is the height (m) from the mean water surface to the ground surface, and h_{ij} is the height (m) from the ground surface to the water surface.

2.3.4. Groundwater Model Theory

The calculation module applied in the GSSHA model is based on the GAR (Green–Ampt Redistribution) approach, which simulates groundwater flow. Green–Ampt infiltration with redistribution (GAR) [33] is particularly effective when there are significant breaks in rainfall events or during continuous simulations.

For fine-textured soils, the GAR method has been shown to produce results very similar to those derived from Richard’s solution [33]. When applied to watersheds identified as Hortonian, the GAR method generates results comparable to those obtained using Richard’s Equation [34].

Infiltration calculated through GAR is used to approximate groundwater recharge in two-dimensional saturated groundwater flow simulations. Groundwater recharge at each time step is computed using the following equation:

$$R = (F^{l+\Delta t} - F^l)A \quad (16)$$

Here, R is equal to the recharge (m^3), F is the total infiltration (m), and A is the area of the overland flow cell (m^2). A simple two-layer soil moisture calculation routine is used to compute soil moisture. If the groundwater elevation exceeds the surface elevation, infiltration calculations for the cell are halted, and groundwater surface exchange is calculated as described earlier. Anytime exfiltration occurs, the infiltration and overland flow processes are initiated if they are not already active. These processes continue as long as infiltration occurs and until all water on the overland surface ceases to flow and infiltrate. Infiltration is not calculated for cells where exfiltration is occurring.

Rivers and groundwater interact through repeated infiltration and exfiltration processes. To account for river–groundwater interactions, the sediment thickness (cm) and hydraulic conductivity (cm/h) values, which represent the thickness of the soil layer through which the flow must pass during the exchange between groundwater and each river section, were applied using the values provided in the Soyang River Master Plan Report for South Korea. Additionally, to consider the flow between the river and the underlying saturated groundwater zone, a river flux was applied to all river sections. The river flux is calculated based on Darcy’s Law, as explained by McDonald et al. (1988) [35]. This ensures smooth water flow and interaction between the river and groundwater. The model simulation concludes after considering all interactions, such as the flow entering the river and then exfiltrating through the groundwater or the groundwater re-entering the river.

$$f = -\frac{K_{rb}}{M_{rb}}(E_r - E_{ws}) \quad (17)$$

Here, f represents the per unit area discharge (m/s), K_{rb} is the hydraulic conductivity of the riverbed material (cm/h), M_{rb} is the depth of the riverbed material (cm), E_r is the elevation of the river water surface (m), and E_{ws} is the elevation of the groundwater water surface (m).

A negative flux indicates flow into the groundwater. When the groundwater surface elevation is lower than the riverbed elevation, the rate at which the river flows into the groundwater is expressed as

$$f = -K_{rb} \quad (18)$$

If the groundwater surface elevation is higher than the water surface elevation of the stream, groundwater exfiltrates into the river. In this case, the flux is positive, representing the flow from the groundwater to the river.

For groundwater simulation using the GSSHA model for the selected watershed, it is essential to input groundwater parameters, spatial distribution data for grid-based aquifer depth, and initial groundwater level data. The input parameters for groundwater simulation include hydraulic conductivity (cm/h) and porosity (m^3/m^3). The GIS-based

raster calculator was utilized to apply the spatial distribution of grid-based aquifer depth and initial groundwater levels.

This study used this function to distribute data spatially based on DEM, calculating and applying the distribution in the order of surface elevation, initial groundwater level, and aquifer depth (EL·m). Different distribution equations were applied according to the methods used for applying the aquifer depth parameter. Initial groundwater levels were applied as percentages based on aquifer depth and elevation. In the final model of the study, the initial groundwater level parameter was spatially distributed to 50% from the deepest aquifer depth to the surface, and aquifer depth varied according to different estimation techniques. The groundwater soil parameters used in this study are shown in Table 5 [36].

Table 5. Parameters of groundwater simulation.

Parameters	Hydraulic Conductivity (cm/h)	Porosity (m ³ /m ³)
Sand	11.78	0.437
Loamy sand	2.99	0.437
Sandy loam	1.09	0.453
Loam	0.66	0.463
Silt loam	0.34	0.501
Sandy clay loam	0.15	0.398
Clay loam	0.10	0.464
Silty clay loam	0.10	0.471
Clay	0.03	0.475

2.3.5. Meteorological Data for Long-Term Simulation

A long-term simulation period that can model the hydrological cycle is necessary for performing groundwater simulations. In this research, a three-year long-term simulation was conducted from January 2018 to December 2020. However, data from 2018 were used for calibrating the hydrological cycle based on the initial conditions of the watershed, while data from January 2019 to December 2020 were used for analyzing long-term simulation results of streamflow and groundwater level calibration and validation. The long-term simulation included meteorological data, spatial and temporal parameters of the target area, and evapotranspiration parameters. The evapotranspiration calculations were performed using the Penman method.

Precipitation is the primary factor influencing natural groundwater recharge in arid regions. In this study, eight observation stations, including one in North Korea, were selected to consider the spatial rainfall distribution in the Soyang River Basin, which includes the North Korean region. The selected stations are seven located in South Korea (Chuncheon, Sokcho, Daegwallyeong, Inje, Myeongae, Sangnam, and Yongdae) and one in North Korea (Jangjeon). Rainfall data for the South Korean stations were obtained from the Korea Meteorological Administration (KMA), the Ministry of Environment (KME), and the Korea Water Resources Corporation (K-water), while rainfall data for North Korea were sourced from the World Meteorological Organization (WMO). Rainfall data from each station were spatially distributed across the watershed using the Inverse Distance Weighting (IDW) method. The specifications and locations of the rain gauge stations are shown in Figure 9 and Table 6.

Other meteorological data, besides rainfall, were hourly data that were provided by the national meteorological station in Chuncheon, where the Soyang River Basin is located. The location of the target area (Longitude 128.265, Latitude 38.041) and the standard time settings were applied to account for factors such as the angle of sunlight and cloud cover. The time difference between Greenwich Mean Time (GMT) and Korea Standard Time (KST) is +9 h. The hourly meteorological data applied in the long-term simulation include atmospheric pressure (Hg), relative humidity (%), wind speed (kts), temperature (F), cloud cover (%), solar radiation (%), and solar radiation energy.

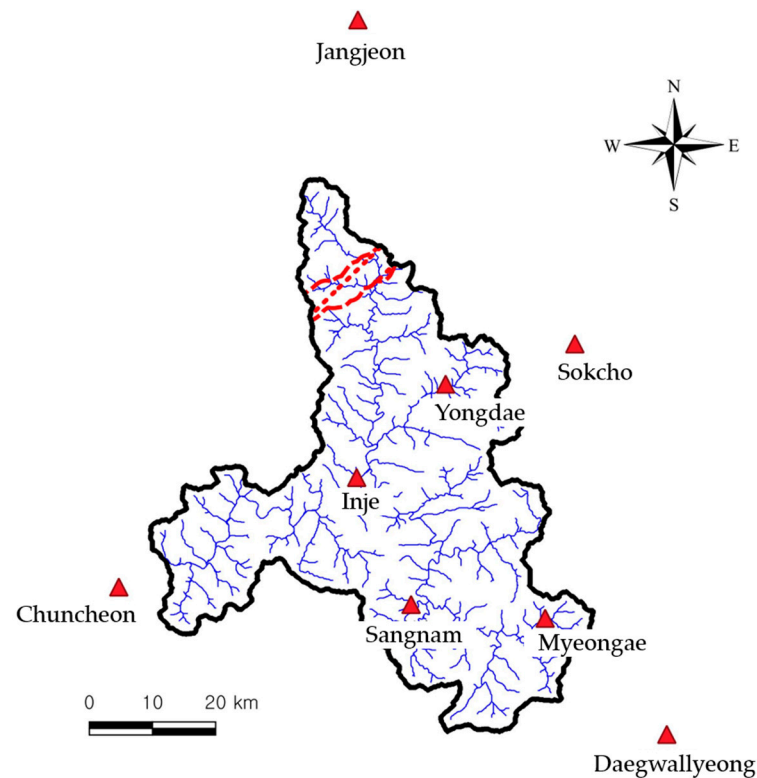


Figure 9. Location of weather gauge stations in the Soyang River Basin.

Table 6. Specification of the weather gauge station.

Country	Station Name	Supervisory Authority	Longitude	Latitude
South Korea	Chuncheon	KMA	127-44-08	37-54-09
	Sokcho	KMA	128-33-52	38-15-03
	Daegwallyeong	KMA	128-43-03	37-40-22
	Inje	KMA	128-10-01	38-03-36
	Myeongae	KME	128-30-12	37-50-60
	Sangnam	K-water	128-15-43	37-52-24
	Yongdae	K-water	128-19-47	38-11-44
North Korea	Jangjeon	WMO	128-12-5	39-33-3

3. Case Study and Results

3.1. Aquifer Depth Estimation Simulation Scenarios

The complexity of aquifer structures due to the mountainous terrain prevalent in South Korea adds challenges to hydrological modeling. The depth of the main groundwater table in an alluvial aquifer becomes slightly deeper toward the river, indicating the overall groundwater flow toward the river [37]. This pattern is also observed in multiple national groundwater survey reports in South Korea, which state that in mountainous areas, groundwater tends to flow at shallow depths as the surface elevation increases, with depths often less than 1 m [38]. Conversely, as the surface elevation decreases and moves toward flatter regions, the groundwater depth tends to increase. To more accurately represent the natural hydrological cycle, aquifer depths calculated using the three equations below were applied to the physically based distributed hydrological model.

The three proposed cases include uniform distribution, linear regression, and logarithmic regression. The three equations were derived based on the surface elevation range of 176 EL-m to 1574 EL-m in the Soyang River Basin and aquifer depth data from the measured points. The aquifer depth in the Chuncheon area, where the Soyang River is located, was

determined using the bedrock aquifer depths provided in the *Groundwater Basic Survey Report for Chuncheon Area* [38], and the regression equations were derived accordingly.

A raster calculation was performed to apply the initial groundwater level and aquifer depth layers in the grid-based physically based hydrological model. Based on the surface elevation of the Soyang River Basin, the elevation of the initial groundwater level and aquifer depth were calculated according to the equations shown in the three cases below. In the equations, x represents the surface elevation of the corresponding grid cell, and y represents the aquifer depth. The initial groundwater level was set to be located in the middle between the aquifer bottom and the surface elevation, and the simulation was conducted accordingly.

3.1.1. Case 1: Uniform Distribution

The uniform distribution scenario applied an aquifer depth of 60 m, which falls within the average depth range of 60 m to 80 m for bedrock aquifers, as suggested by the groundwater survey report of the Chuncheon area [38]. This simple calculation method assumes that the aquifer is uniformly distributed at 60 m below the surface elevation for all grid cells. In Equations (19)–(21), x represents the surface elevation (EL·m), and y represents the aquifer bottom (EL·m). The equation for applying the aquifer depth parameter in this uniform distribution scenario is as follows:

$$y = x - 60(\text{m}) \quad (19)$$

3.1.2. Case 2: Linear Regression

In this study, to account for variations in aquifer depth with elevation, the minimum and maximum depths were established, and aquifer depths of all elevations were represented using a linear inverse relationship. The aquifer depth of the lowest elevation area in the Soyang River Basin (176 EL·m) was set to 100 m, deeper than the average bedrock aquifer depth of 60 m in the Chuncheon area. Conversely, the aquifer depth of the highest elevation area (1574 EL·m) was set to 0.5 m. These values of 100 m and 0.5 m were established based on domestic aquifer depth survey data provided by the National Geographic Information Institute of Korea (NGII) [39,40]. The linear regression equation derived from this approach is as follows:

$$y = -0.0711x + 112.52 \quad (20)$$

3.1.3. Case 3: Logarithmic Regression

Building on the linear regression scenario from Section 3.1.2, this study transformed the trendline into a logarithmic regression equation under the same conditions. The logarithmic regression can reveal more extreme values compared to the linear regression. With the same conditions of a maximum aquifer depth of 100 m and a minimum depth of 0.5 m, the linear regression graph shows a straight line, while the logarithmic regression graph forms a curve. The logarithmic regression graph shows an aquifer depth range from a minimum of 18 m to a maximum of 122 m. Compared to the linear regression graph, there is a difference of approximately 17.5 m at the highest elevation and about 22 m at the lowest elevation. The coefficient of determination (R^2) for the logarithmic regression is 0.933 [41]. The logarithmic regression equation is as follows:

$$y = -49.02\ln(x) + 375.65 \quad (21)$$

3.2. Calibration and Validation

3.2.1. Procedures for Calibrating and Validating

Calibration and validation are essential processes in hydrological modeling. For physical models like GSSHA, when conducting long-term simulations that cover an extensive period, setting the calibration period before the period of interest allows the model to natu-

rally reproduce hydrological processes and adjust parameters closer to reality. However, when precise groundwater simulations are included, the time required for replicating these hydrological cycles increases significantly due to the much slower hydraulic conductivity within subsurface pores compared to surface flow velocities.

Other methods for parameter calibration include manual techniques such as trial-and-error and the GSSHA automatic calibration method. However, the results obtained from automatic calibration methods can sometimes yield parameters or predictions that are difficult for hydrologists to accept, which is why these methods are not widely used in hydrological or water quality models (Boyle et al., 2000) [42]. Instead, manual calibration techniques, which may take longer but can produce better calibration results, are used in many studies (Madsen, 2000) [43]. Therefore, this study employed a method in which one factor at a time was adjusted for parameter calibration.

Hong et al. (2010) conducted a sensitivity analysis of a distributed model in the terrain of South Korea and indicated that the initial saturation of soil and groundwater, as well as the river roughness coefficient, should be prioritized in parameter calibration [44]. Similarly, the sensitivity analysis of the parameters applied to the GSSHA model showed that the parameters involved in the infiltration processes of groundwater and soil had high sensitivity, consistent with the findings of Hong et al. (2010) [44]. The calibration parameters and the order of calibration are presented in Table 7.

Table 7. Calibration target parameters, scope, and calibration order.

Calibration Order	Calibration Target Parameters	Parameters Range
1	Initial ground water level (%)	30–80
2	Constant head groundwater level (%)	30–70
3	Infiltration parameters	-
4	Surface roughness coefficient	0.0137–0.4
5	Channel width (m)	3–800

This study used eight error evaluation methods to assess the suitability of the constructed model in various aspects such as trends, peak flow, and total runoff volume. The stream flow for each aquifer depth estimation scenario in the Soyang River Basin was compared and analyzed. The model's suitability and correlation were evaluated using functions such as the coefficient of determination, the R-squared statistic (R^2), root mean square error (RMSE), Nash–Sutcliffe Efficiency index (NSE) [45], and relative mean absolute error (RMAE). Additionally, The relative volume error (RVE) and relative peak error (RPE) were used to assess how well the model simulates volume and peak flow. The Index of Agreement measure (IoAd), proposed by [46], represents the regression relationship between simulated and observed values, while the correlation coefficient (CC) indicates the strength of the linear relationship between the two values based on their variance patterns [47]. We classified the coefficient of determination (R^2) range into four categories, namely, very good, good, fair, and poor, to evaluate the model's suitability. Formulas and descriptions for each error evaluation metric are provided in Table 8.

- Q_0 : Observed discharge values;
- Q_g : Estimated discharge;
- $\overline{Q_0}$: Mean observed discharge;
- $\overline{Q_g}$: Mean estimated discharge;
- Q_{0p} : Peak observed discharge;
- Q_{gp} : Peak estimated discharge;
- n : Number of data;
- σ : Standard deviation of observed values.

Table 8. Formulas and description of error evaluation metrics.

Error Evaluation Metrics	Formula	Description
RMSE	$\sqrt{\frac{\sum_{i=1}^n (Q_0 - Q_g)^2}{n}}$	Relative error, $\sim \infty$
RMAE	$\frac{\frac{1}{n} \sum_{i=1}^n Q_g - Q_0 }{Q_0}$	Relative mean error, $\sim \infty$
RVE	$\frac{\sum_{i=1}^n (Q_g - Q_0)}{\sum_{i=1}^n Q_0}$	Closer to 0 is better, $-1 < RVE < 1$
RPE (%)	$\frac{ Q_{0p} - Q_{gp} }{Q_{0p}} \times 100$	Smaller is better, RPE < 100 (%)
R ²	$\left[\frac{\sum_{i=1}^n (Q_0 - \bar{Q}_0) \times (Q_g - \bar{Q}_g)}{\sum_{i=1}^n (Q_0 - \bar{Q}_0)^2 \times \sum_{i=1}^n (Q_g - \bar{Q}_g)^2} \right]^2$	0.8 ≤ R ² < 1 (very good), 0.7 ≤ R ² < 0.8 (good), 0.6 ≤ R ² < 0.7 (fair), R ² < 0.7 (poor)
NSE	$1 - \frac{\sum_{i=1}^n [Q_0 - Q_g]^2}{\sum_{i=1}^n [Q_0 - \bar{Q}_0]^2}$	0.8 ≤ NSE < 1 (very good), 0.7 ≤ NSE < 0.8 (good) NSE < 0.7 (poor)
IoAd	$1 - \frac{\sum_{i=1}^n (Q_g - Q_0)^2}{\sum_{i=1}^n (Q_g - \bar{Q}_g + Q_0 - \bar{Q}_0)^2}$	Closer to 1 is better
CC	$\frac{n \times \sum_{i=1}^n Q_g \times Q_0 - (\sum_{i=1}^n Q_g) \times (\sum_{i=1}^n Q_0)}{\sqrt{[n \times \sum_{i=1}^n Q_g^2 - (\sum_{i=1}^n Q_g)^2] \times [n \times \sum_{i=1}^n Q_0^2 - (\sum_{i=1}^n Q_0)^2]}}$	Closer to 1 is better

3.2.2. Details of Groundwater Simulation Validation

Among the various methods for estimating groundwater recharge, there is the water table fluctuation (WTF) method, which uses data from groundwater monitoring wells [48]. In this study, simulation points were created to correspond to the actual locations of six groundwater observation wells (Chuncheon–Buksan, Inje–Nammyeon, Inje–Inje, Inje–Wontong, Inje–Guidun, Inje–Girin) to verify the groundwater level results for each scenario. Calibration and validation processes were conducted to obtain reliable results. However, as each grid’s representative elevation is input into the model, there are considerable distortions from the actual topographic elevations. It is technically challenging to apply the exact elevations of the groundwater observation wells to specific points within the model. In terrain distributed in grid form, the grid size causes a smoothing effect, resulting in elevations that may be higher or lower than the actual terrain. Therefore, the simulated groundwater level results for each scenario were adjusted by comparing them with the observed groundwater-level data. Error evaluation indices and trend graphs were compared based on these adjusted simulated values. The error indices were derived from the simulated groundwater level variations by elevation. The trend comparison graphs included, first, graphs showing groundwater level fluctuations by elevation over the simulation period, and second, graphs showing groundwater level changes over the simulation period.

Additionally, among the observation data used for model validation, the Inje–Wontong observation station is located close to the center of the main river. This proximity may result in frequent and complex stream–groundwater interactions, such as infiltration and exfiltration from the riverbed, leading to a highly intricate groundwater flow system.

In this research, a two-year simulation of groundwater fluctuation was conducted to validate the aquifer depth estimation methods applicable to the distributed model, and six groundwater observation wells within the study area were selected. The locations of the groundwater observation wells are shown in Figure 10. Due to their proximity to the river, it is likely that river stage fluctuations significantly influence groundwater level variations. To precisely account for groundwater level changes in hydrological models, a more detailed consideration of hydrological parameters associated with processes occurring at the riverbed is required. However, as this study’s primary focus was on identifying optimal

methods for aquifer depth distribution, rather than detailed groundwater investigations, such analyses were beyond its scope but warrant further exploration.

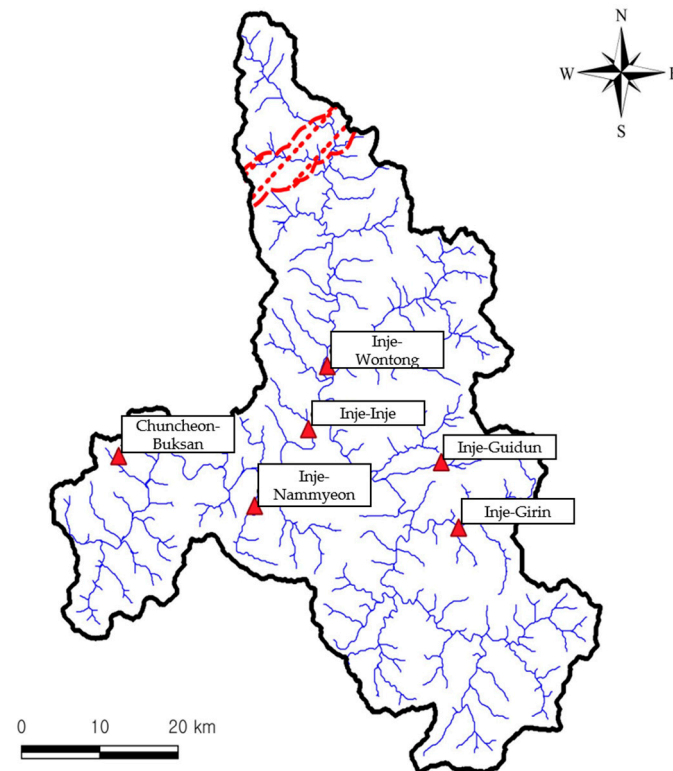


Figure 10. Location of groundwater observation wells in the Soyang River Basin.

Furthermore, the six groundwater observation wells selected for this study were based on data from the National Groundwater Monitoring Network. As a result, observation wells located in areas less influenced by the river were not included, which represents a limitation of this study. This limitation highlights the need for future research to incorporate more diverse monitoring sites to better assess river–groundwater interactions under varying conditions.

The study compared curves of the observed groundwater level from the groundwater observation wells with curves of the simulated groundwater level from the model, using different methods of estimating aquifer depth. The trend comparison graphs included the groundwater level fluctuation by elevation and the change in groundwater level over the simulation period. Furthermore, error evaluation indices were based on the simulated groundwater level variations by elevation.

For the error evaluation, five metrics (RMSE, RMAE, R^2 , IoAd, CC) were used to access groundwater levels. The applicability of the aquifer depth estimation methods was evaluated by considering the trends in groundwater level fluctuation, the magnitude and average of errors, and the efficiency of the model. Error evaluation of the model was conducted by comparing the groundwater level data from each observation well in the Soyang River Basin with the corresponding simulated groundwater levels.

3.3. Stream Flow Results

The error evaluation results for the three methods showed that RPE was most favorable in Case 3, which applied logarithmic regression. RVE, indicating the degree of under- or over-simulation, showed the best results for the linear regression method. Furthermore, RMSE and RMAE, which represent the magnitude and average of errors, respectively, were most favorable for the logarithmic regression method. NSE and R^2 , indicating the model's efficiency, were highest for the linear regression method, followed by the logarithmic

regression and uniform distribution methods. The error evaluation results for each scenario in the Soyang River Basin are summarized in Table 9, and the graphs comparing the observed and simulated hydrographs are shown in Figures 11–13.

Table 9. Error evaluation results for flow simulated at different aquifer depths.

Error Evaluation Metrics	Case 1 (Uniform)	Case 2 (Linear)	Case 3 (Logarithmic)
RMSE	0.716	0.667	0.722
RMAE	0.406	0.467	0.517
RVE	−0.126	0.076	0.193
RPE (%)	5.553	10.547	4.902
R ²	0.830	0.858	0.838
NSE	0.693	0.789	0.751
IoAd	0.840	0.948	0.939
CC	0.934	0.915	0.901

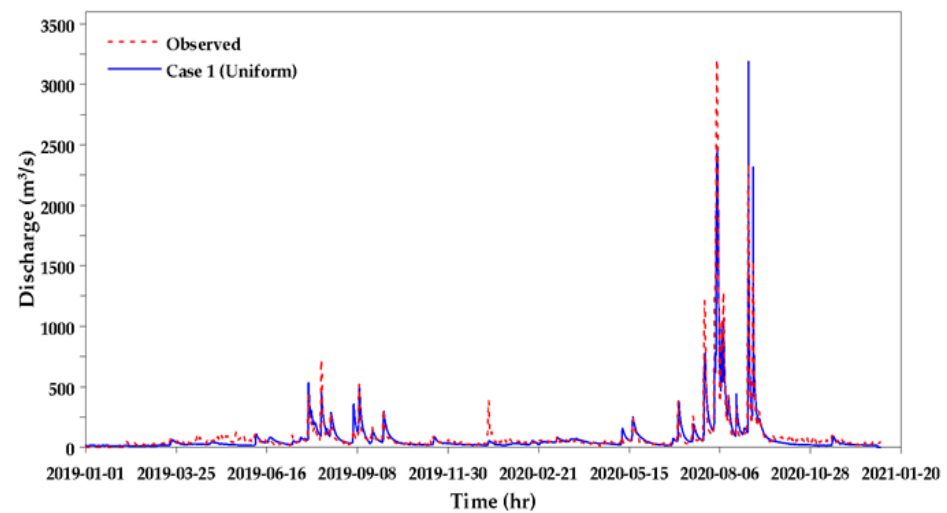


Figure 11. Comparison of simulated and observed runoff hydrographs for Case 1, based on uniform distribution.

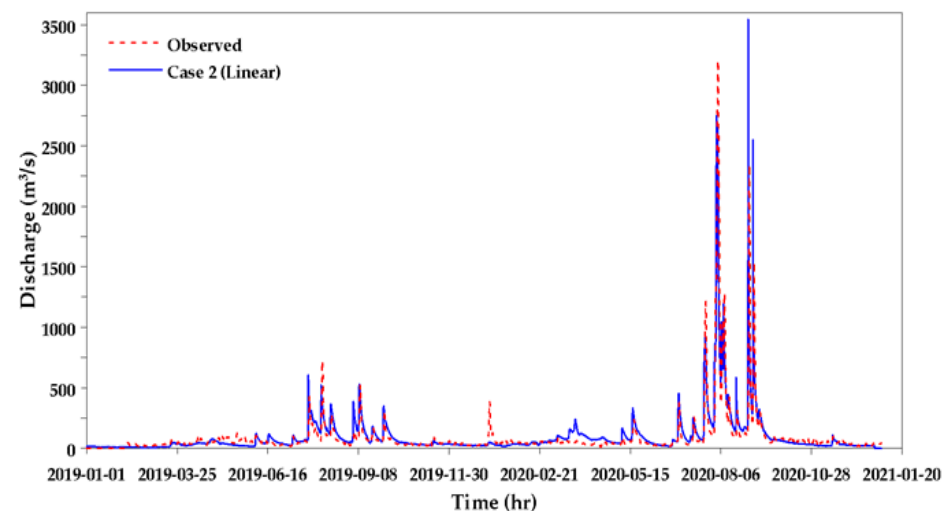


Figure 12. Comparison of simulated and observed runoff hydrographs for Case 2, based on linear regression.

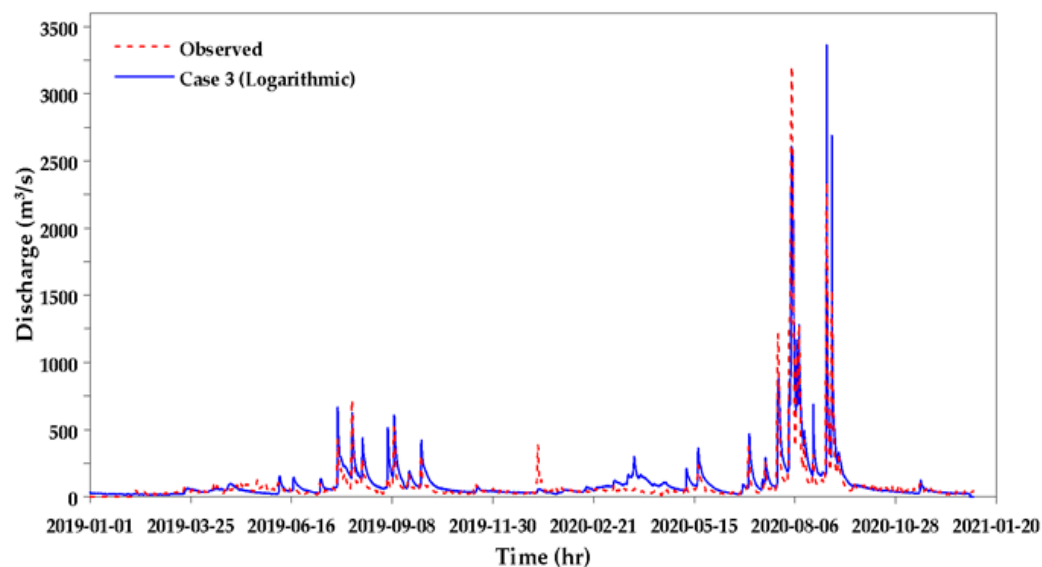


Figure 13. Comparison of simulated and observed runoff hydrographs for Case 3, based on logarithmic regression.

The simulation results for runoff in the Soyang River Basin, using the uniform distribution method, showed a peak flow of $3187.32 \text{ m}^3/\text{s}$, which is $17.72 \text{ m}^3/\text{s}$ lower than the observed peak flow of $3205.04 \text{ m}^3/\text{s}$, indicating a slight underestimation. The RPE was 5.553%, suggesting that the simulated value accurately reflects the observed peak flow. Additionally, the RVE index was -0.126 , indicating that the overall simulation results slightly underestimated the observed values. The RMSE was 0.716, and the RMAE was 0.406, while the R^2 and NSE indicated that the model's efficiency is generally excellent.

The simulation results for runoff in the Soyang River Basin using the linear regression method showed a peak flow of $3543.07 \text{ m}^3/\text{s}$, which is $338.03 \text{ m}^3/\text{s}$ higher than the observed peak flow of $3205.04 \text{ m}^3/\text{s}$, indicating an overestimation. The RPE was 10.547%, suggesting that the simulated value reflects the observed value reasonably well. The RVE index was 0.76, indicating that the overall simulation results slightly overestimated the observed values. The RMSE was 0.667, and the RMAE was 0.467, showing relatively small errors. Both NSE (0.789) and R^2 (0.858) ranged from good to very good, indicating that the model's efficiency is generally favorable.

The simulation results for runoff in the Soyang River Basin using the logarithmic regression method showed a peak flow of $3362.15 \text{ m}^3/\text{s}$, which is $157.11 \text{ m}^3/\text{s}$ higher than the observed peak flow of $3205.04 \text{ m}^3/\text{s}$, indicating an overestimation. The RPE was 4.902%, suggesting that the simulated values closely reflect the observed values. The RVE was 0.193, indicating that the simulated values were slightly higher than the observed ones. The errors were RMSE 0.722 and RMAE 0.517. The model's efficiency indicators, NSE (0.751) and R^2 (0.838), were all analyzed as good (0.751) to very good (0.838). Additionally, other indicators such as IoAd and CC were also analyzed favorably, indicating that the regression relationship between the simulated and observed values is largely excellent.

3.4. Groundwater Level Simulation Results

Groundwater level error evaluation was conducted using water level data from the Chuncheon–Buksan observation well, located in the downstream area of the Soyang River Basin. The RMSE and RMAE, which represent the magnitude and average of errors, respectively, showed similar results across all three aquifer depth estimation methods (Case 1, Case 2, and Case 3). The coefficient of determination (R^2), which indicates the model's efficiency, also brought out similar results for all three cases. This is likely because the Chuncheon–Buksan observation well is situated at the lowest part of the basin, where there was minimal difference in the aquifer depth applied. No significant differences

were observed in other evaluation metrics either. The detailed results for each metric are presented in Table 10, and the graph comparing the observed and simulated groundwater levels is shown in Figure 14.

Table 10. Error evaluation results at Chuncheon–Buksan observation station.

Error Evaluation	Case 1 (Uniform)	Case 2 (Linear)	Case 3 (Logarithmic)
RMSE	0.0034	0.0035	0.0034
RMAE	0.0003	0.0002	0.0003
R ²	0.6776	0.6721	0.6760
IoAd	0.7998	0.8024	0.7991
CC	0.7580	0.7396	0.7573

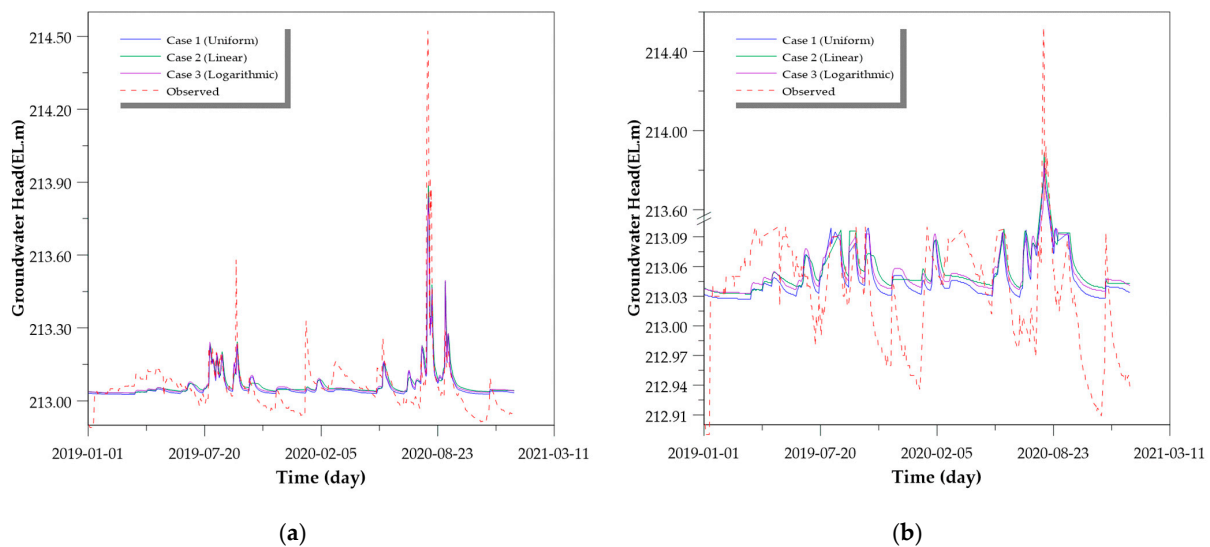


Figure 14. Chuncheon–Buksan: observed and simulated groundwater levels. (a) Original groundwater levels; (b) groundwater levels with y-axis break.

Groundwater level error evaluation was conducted using data from the Inje–Nammyeon observation well, located in the downstream area of the basin. The RMSE and RMAE were smallest for Case 3 (logarithmic), followed by Case 2 (linear), and then Case 1 (uniform). However, there was no significant difference between Case 3 and Case 2, with RMSEs of 0.0155 and 0.0151, respectively. When evaluating the efficiency of each method based on R², Case 3 resulted in a value of 0.5487, while Case 2 yielded 0.5478, exposing the least difference. Case 1 showed the lowest efficiency with a value of 0.5237. In terms of IoAd, Case 2 produced the best results, followed by Case 3 and Case 1. For the CC metric, Case 3 showed the best performance, followed by Case 2 and Case 1, with Case 1 being the least efficient. The detailed results for each metric are presented in Table 11, and the graph comparing the observed and simulated groundwater levels is shown in Figure 15.

Table 11. Error evaluation results at Inje–Nammyeon observation station.

Error Evaluation	Case 1 (Uniform)	Case 2 (Linear)	Case 3 (Logarithmic)
RMSE	0.0235	0.0155	0.0151
RMAE	0.0027	0.0013	0.0013
R ²	0.5237	0.5478	0.5487
IoAd	0.4852	0.5282	0.5234
CC	0.7593	0.8204	0.8275

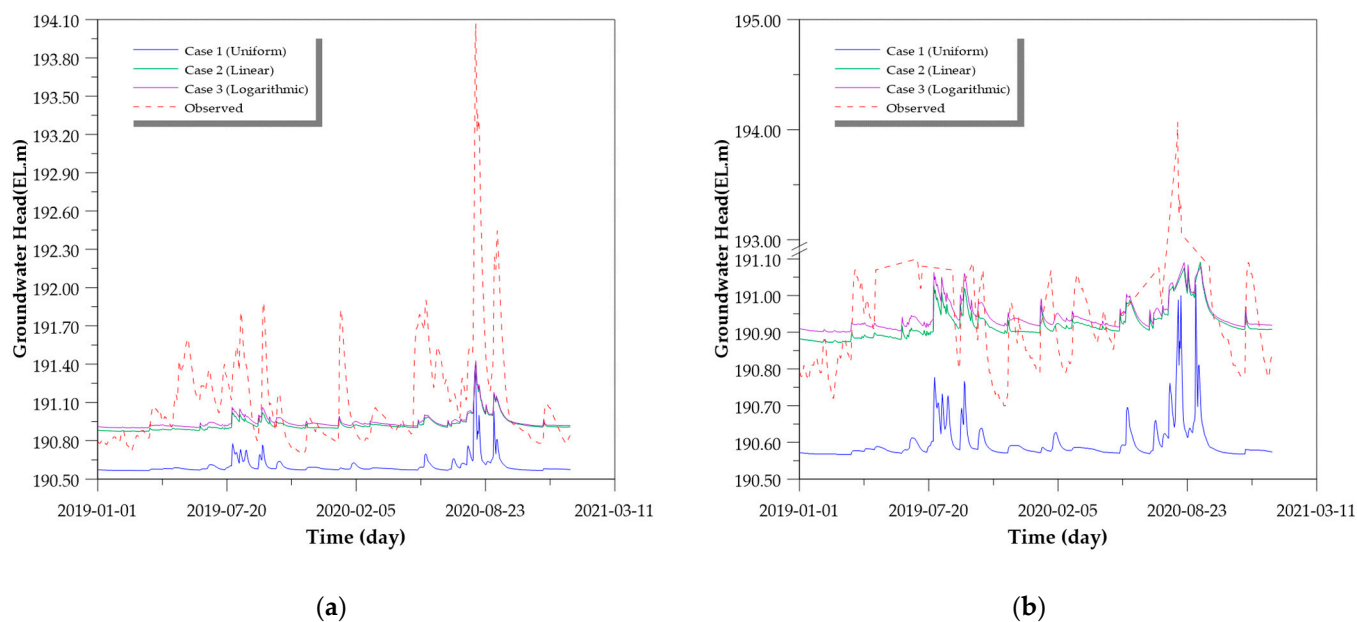


Figure 15. Inje–Nammyeon: observed and simulated groundwater levels. (a) Original groundwater levels; (b) groundwater levels with y-axis break.

Error evaluation of groundwater level by aquifer depth estimation methods at the Inje–Inje observation well revealed that RMSE and RMAE did not expose significant differences across the three cases. The R^2 values indicated high efficiency for all three cases, with Case 2 bearing the best result at 0.7112, followed by Case 3 at 0.7062, and Case 1 at 0.6982. The IoAd results were similarly favorable, with Case 2 at 0.8553, Case 3 at 0.8448, and Case 1 at 0.8393. The CC metric also reflected this trend, with Case 2 at 0.9089, Case 3 at 0.8869, and Case 1 at 0.8866. Notably, the CC value, which demonstrates correlation, was exceptionally high, giving it the most favorable result among all observation wells in the basin. The precise results for each metric at Inje–inje are presented in Table 12, and the graph comparing the observed and simulated groundwater levels is laid out in Figure 16.

Table 12. Error evaluation results at Inje–Inje observation station.

Error Evaluation	Case 1 (Uniform)	Case 2 (Linear)	Case 3 (Logarithmic)
RMSE	0.0101	0.0100	0.0098
RMAE	0.0009	0.0009	0.0009
R^2	0.6982	0.7112	0.7062
IoAd	0.8393	0.8533	0.8448
CC	0.8866	0.9089	0.8869

The Inje–Wontong observation station, located in the central part of the watershed, had the least favorable error evaluation results among all observation stations in the watershed. Additionally, the measurements of groundwater level at this station showed significant differences in the pattern of changes in level compared to nearby stations within the watershed. This discrepancy was likely due to the station’s proximity to the center of the main river, unlike the other stations. The interaction between the river and groundwater, such as infiltration from the riverbed and groundwater exfiltration during river level drops, can occur frequently, leading to a highly complex groundwater flow system.

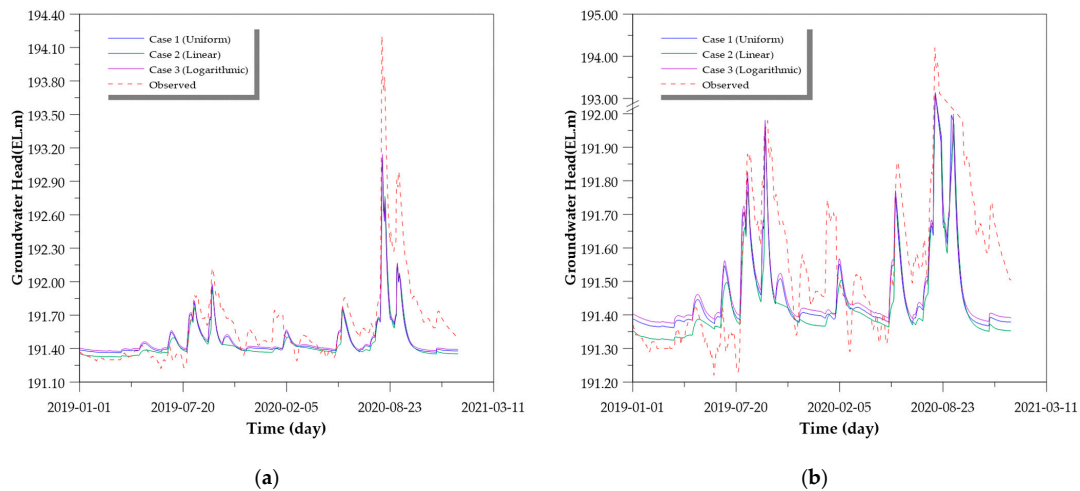


Figure 16. Inje–Inje: observed and simulated groundwater levels. (a) Original groundwater levels; (b) groundwater levels with y-axis break.

Results of the error evaluation of the aquifer depth estimation methods at the Inje–Wontong station revealed no significant differences in RMSE and RMAE. The R^2 values for all three cases were analyzed to be very similar. The IoAd, another error evaluation indicator, showed results of 0.676 for Case 1, 0.6548 for Case 3, and 0.5948 for Case 2, indicating that Case 1 and Case 3 provided better results. Similar outcomes were observed in the CC, where Case 1 was found to be the most efficient, albeit with a slight margin. Table 13 presents the error evaluation results for each method, and Figure 17 compares the measured groundwater level graph with the simulated groundwater level graph at the Inje–Wontong station.

Table 13. Error evaluation results at Inje–Wontong observation station.

Error Evaluation	Case 1 (Uniform)	Case 2 (Linear)	Case 3 (Logarithmic)
RMSE	0.0596	0.0570	0.0582
RMAE	0.0029	0.0031	0.0030
R^2	0.5378	0.5393	0.5376
IoAd	0.6760	0.5948	0.6548
CC	0.4047	0.3954	0.3992

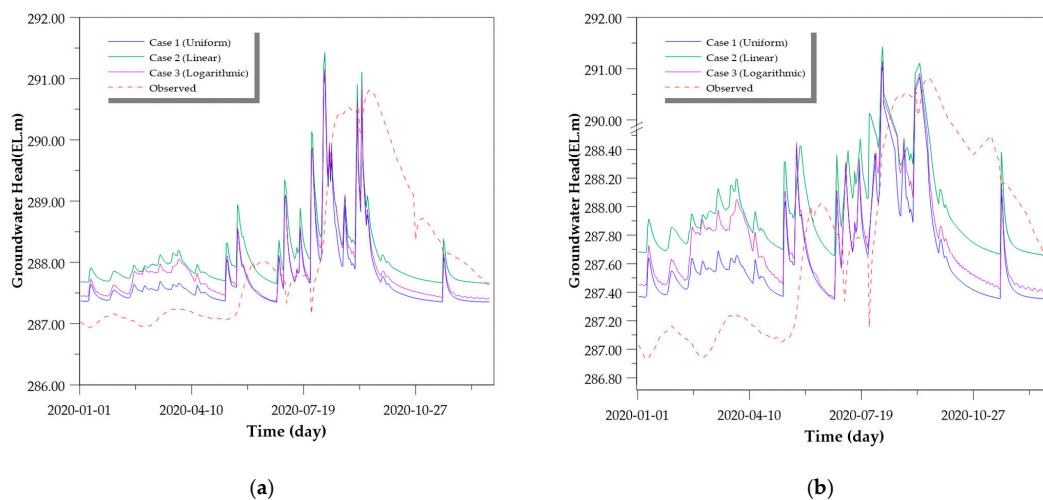


Figure 17. Inje–Wontong: observed and simulated groundwater levels. (a) Original groundwater levels; (b) groundwater levels with x- and y-axis breaks.

The Inje–Guidun observation station is in the upper part of the watershed, which is closer to mountainous terrain, and in an area where the elevation gradually increases within the watershed. The error evaluation results for this station showed that the RMSE was the best for Case 2, followed by Case 1 and then Case 3. No significant differences were observed in the RMAE. Regarding R^2 , Case 2 produced the best results, while Cases 3 and 1 were analyzed at similar levels. Other indicators, such as IoAd and CC, were analyzed at satisfactory levels. The application of Case 2 provided the most stable results. The outcome of error evaluation for the Inje–Guidun observation station are presented in Table 14, and the graph comparing the observed groundwater levels with the simulated groundwater levels is shown in Figure 18.

Table 14. Error evaluation results at Inje–Guidun observation station.

Error Evaluation	Case 1 (Uniform)	Case 2 (Linear)	Case 3 (Logarithmic)
RMSE	0.0156	0.0139	0.0171
RMAE	0.0006	0.0006	0.0006
R^2	0.6423	0.6818	0.6400
IoAd	0.8638	0.8004	0.6928
CC	0.7826	0.8436	0.8369

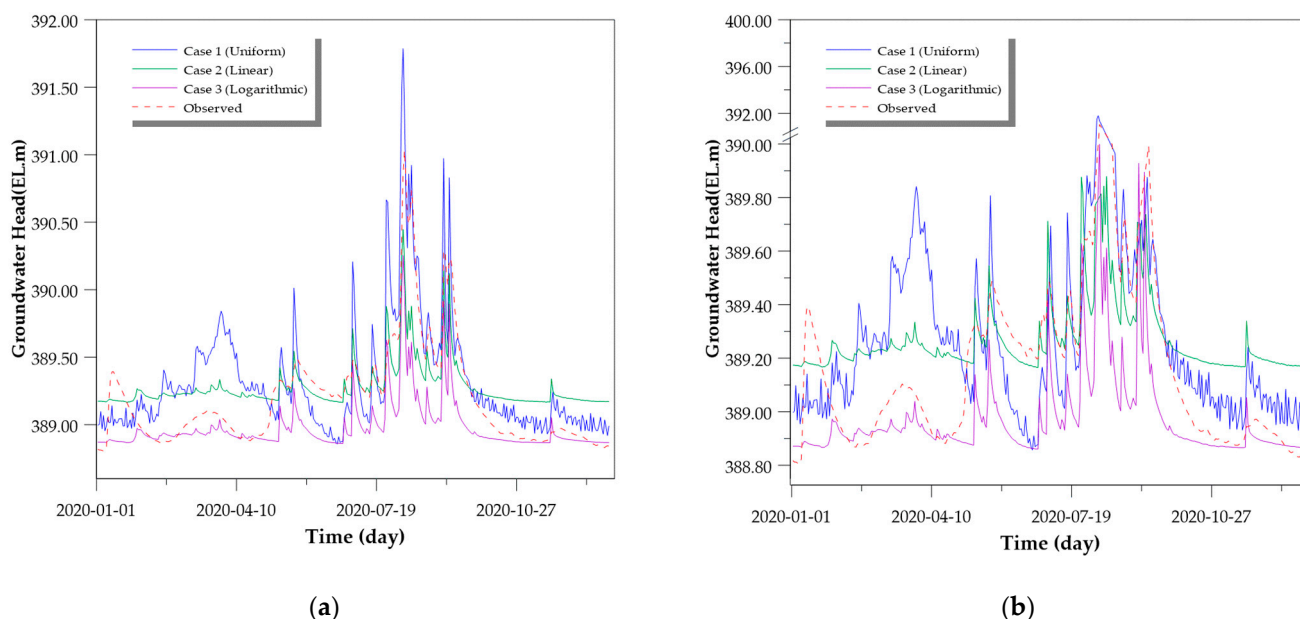


Figure 18. Inje–Guidun: observed and simulated groundwater levels. (a) Original groundwater levels; (b) groundwater levels with x- and y-axis breaks.

The Inje–Girin observation station is in the upper part of the Soyang River Basin, with a high distribution of mountainous terrain. The RMSE results were best for the uniform distribution at 0.0061, followed by linear regression at 0.0067, and log regression at 0.0176. The R^2 values were effective for the log and uniform distribution methods, but the linear regression method produced somewhat lower results. The IoAd designated that the uniform distribution and linear regression methods produced favorable results, whereas the log regression did not perform as well. The CC metric confirmed satisfactory results for all three methods. The error evaluation results of the three methods conducted at the Inje–Girin observation station are presented in Table 15, and Figure 19 graphically compares the observed groundwater levels with the simulated groundwater levels.

Table 15. Error evaluation results at Inje–Girin observation station.

Error Evaluation	Case 1 (Uniform)	Case 2 (Linear)	Case 3 (Logarithmic)
RMSE	0.0061	0.0067	0.0176
RMAE	0.0003	0.0003	0.0013
R ²	0.5115	0.4564	0.5178
IoAd	0.8253	0.8086	0.4407
CC	0.7776	0.7672	0.7835

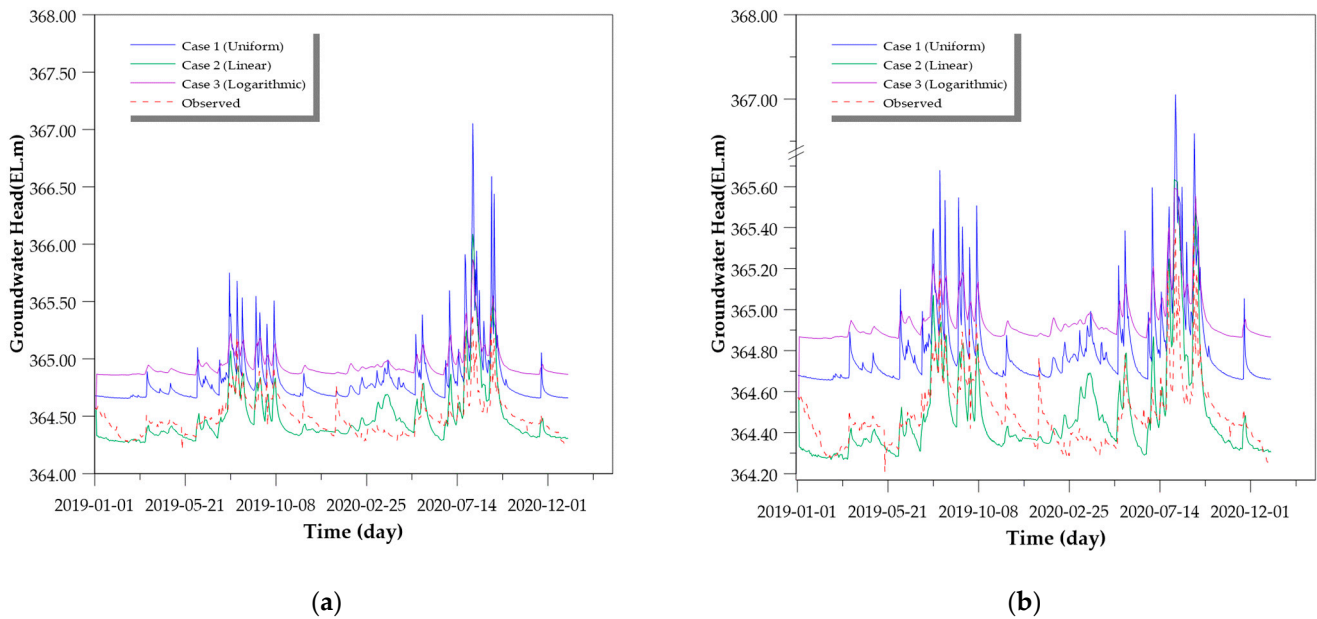


Figure 19. Inje–Girin: observed and simulated groundwater levels. (a) Original groundwater levels; (b) groundwater levels with y-axis break.

4. Conclusions and Future Research

The model employed in this research is the GSSHA distributed model, and three scenarios for estimating aquifer depth parameters were selected and rigorously compared. To account for the complex flow characteristics of groundwater that flows at various depths, which is suitable for simulating the mountainous terrain prevalent in South Korea, the Soyang River Basin was selected as the study area, as it well reflects the topographical characteristics of the country. A long-term simulation was conducted over a three-year period, from 2018 to 2020. The first year of the simulation period was designated as the calibration period for the model, while the latter two years were set as the validation period.

Since the Soyang River Basin includes the upstream region of North Korea along the DMZ, the soil properties were combined with the soil characteristics of North Korea, which were previously compiled for military purposes, based on the soil series codes of South Korea. The soil profile was systematically divided into three layers based on depth. The physical parameters for each layer were then applied according to soil texture, effectively simulating the infiltration process and groundwater flow.

The long-term runoff calculation results for the model during the simulation period showed good performance across all cases, with the regression relationship between simulated and observed values indicated by R² (0.858) and NSE (0.789), revealing that Case 2 performed best, followed by Case 3 with an R² (0.838) that was also satisfactory. The RPE, which evaluates the error in peak flow, was found to be best in Case 3, while the RVE for evaluating the error in total runoff volume was 0.076, and the relative error RMSE was 0.667, confirming the best results in Case 2 (linear).

The results for groundwater level simulation confirmed similar patterns to the observed curves at six observation wells, except for Inje–Wontong. The outcomes for the observation wells located in complex mountainous regions, such as Inje–Nammyeon and Inje–Guidun, showed favorable results for Case 2 (linear) and Case 3 (logarithmic). However, in areas with gentle slopes and closer to downstream regions, the results for all three cases were somewhat unstable, with Case 1 (uniform) demonstrating a consistent difference in groundwater levels compared to observed values. These findings suggest that Case 1, which distributes the aquifer uniformly from the surface, fails to reflect the actual aquifer elevation. When the aquifer elevation is misapplied in watershed modeling, it can significantly affect river–groundwater interactions and groundwater discharge phenomena. This error likely contributed to the lower RVE indicator found in the runoff simulation results for Case 1.

The trends in groundwater level fluctuations were effectively analyzed by all three methods. However, discrepancies between the actual aquifer depth and the estimated aquifer depth in each case resulted in consistent error magnitudes at certain observation sites throughout the simulation period. Additionally, it is assumed that significant errors in aquifer depth exist in grid areas where no observation points are available.

These results suggest that when applying physically based distributed models in regions with significant elevation changes, adjusting aquifer depth according to terrain elevation is more appropriate than the conventional method of uniform distribution. Nevertheless, this study’s reliance on estimated aquifer depth distributions highlights the need for further research into methods that can provide more physically grounded estimates.

Furthermore, due to the inherent complexity of establishing a physically based distributed model, the simulation period was limited to 2–3 years due to the inherent complexity of establishing a physically based distributed model. This duration was not sufficient for the model to independently carry out the calibration process for certain parameters. In future research, we plan to extend the simulation period to 10 years, enabling the model to independently calibrate parameters such as soil saturation and initial groundwater conditions, thereby aiming to more accurately represent the physical hydrological cycle processes.

Author Contributions: All authors substantially contributed to conceiving and designing the research and realizing this manuscript. Conceptualization, C.J. and J.S.; methodology, C.J. and J.S.; software, J.S.; validation, B.K., J.J. and S.C.; formal analysis, J.S.; investigation, B.K., J.J. and S.C.; resources, B.K., J.J. and S.C.; data curation, B.K., J.J. and S.C.; writing—original draft preparation, J.S.; writing—review and editing, C.J.; visualization, J.S.; supervision, C.J.; project administration, C.J.; funding acquisition, C.J. All authors have read and agreed to the published version of the manuscript.

Funding: This research was supported by a Korea Agency for Infrastructure Technology Advancement (KAIA) grant funded by the Korean government (MOLIT) (RS-2023-00250434).

Data Availability Statement: Data are contained within the article.

Conflicts of Interest: The authors declare no conflicts of interest.

References

1. Gardner-Outlaw, T.; Engelman, R. Sustaining water easing scarcity: A second update Revised Data for the Population Action International Report, Sustaining Water. In *Population and the Future of Renewable Water Supplies*; Population Action International: Washington, DC, USA, 1997.
2. Fronzi, D.; Narang, G.; Galdelli, A.; Pepi, A.; Mancini, A.; Tazioli, A. Towards Groundwater-Level Prediction Using Prophet Forecasting Method by Exploiting a High-Resolution Hydrogeological Monitoring System. *Water* **2024**, *16*, 152. [[CrossRef](#)]
3. Jung, J.H. Decision of Hydraulic Special Indices of Unconfined Aquifer Using Pumping Characteristic Curve. Master’s Thesis, University of Kongju, Gongju, Republic of Korea, 2023.
4. Lee, E.S. Ground Water Sustainability and Ground Water-Surface Interaction. *J. Geol. Soc. Korea* **2004**, *40*, 361–368.
5. Yoon, T.H. A Study on the Spatial Distribution of Aquifer Bottom Parameter for GSSHA Model Groundwater Simulation. Master’s Thesis, University of Daejin, Pocheon, Republic of Korea, 2023.
6. Choi, Y.S.; Kim, K.T.; Shim, M.P. Discharge Estimation at Ungauged Catchment Using Distributed Rainfall-Runoff Model. *J. Korea Water Resour.* **2010**, *43*, 353–365. [[CrossRef](#)]

7. Lee, M.H.; Yoo, D.H. Development and Application of Diffusion Wave-based Distributed Runoff Model. *J. Korea Water Resour.* **2011**, *44*, 553–563. [[CrossRef](#)]
8. Lee, M.H. A Study of a Distributed Flood Runoff Model for Its Application. Ph.D. Thesis, University of Ajou, Suwon, Republic of Korea, 2010.
9. Yue, J.; Zhou, L.J.; Du, J.; Zhou, C.; Nimai, S.; Wu, L.; Ao, T. Runoff Simulation in Data-Scarce Alpine Regions: Comparative Analysis Based on LSTM and Physically Based Models. *Water* **2024**, *16*, 2161. [[CrossRef](#)]
10. Paudel, M.; Nelson, E.J.; Downer, C.W.; Hotchkiss, R. Comparing the capability of distributed and lumped hydrologic models for analyzing the effects of land use change. *J. Hydroinform.* **2011**, *13*, 461–473. [[CrossRef](#)]
11. Jang, S.H.; Oh, K.D.; Jo, J.W. Application of the GSSHA model for the long-term simulation of discharge and water quality at the Peace dam. *J. Korea Water Resour.* **2020**, *53*, 357–367. [[CrossRef](#)]
12. Zhang, H.; Rui, X.; Zhou, Y.; Sun, W.; Xie, W.; Gao, C.; Ren, Y. Analysis of the Response of Shallow Groundwater Levels to Precipitation Based on Different Wavelet Scales—A Case Study of the Datong Basin, Shanxi. *Water* **2024**, *16*, 2920. [[CrossRef](#)]
13. Pinder, G.F.; Bredehoeft, J.D. Application of the Digital Computer for Aquifer Evaluation. *Water Resour. Res.* **1968**, *4*, 1069–1093. [[CrossRef](#)]
14. Golmohammadi, G.; Prasher, S.; Madani, A.; Rudra, R. Evaluating Three Hydrological Distributed Watershed Models: MIKE-SHE, APEX, SWAT. *Hydrology* **2014**, *1*, 20–39. [[CrossRef](#)]
15. Chung, I.M.; Kim, Y.J.; Kim, N.W. Estimating the Temporal Distribution of Groundwater Recharge by Using the Transient Water Table Fluctuation Method and Watershed Hydrologic Model. *Appl. Eng. Agric.* **2021**, *37*, 95–104. [[CrossRef](#)]
16. Ware, H.H.; Mengistu, T.D.; Yifru, B.A.; Chang, S.W.; Chung, I.M. Assessment of Spatiotemporal Groundwater Recharge Distribution Using SWAT-MODFLOW Model and Transient Water Table Fluctuation Method. *Water* **2023**, *15*, 2112. [[CrossRef](#)]
17. Shin, J.W. Differences in Flood Runoff Regarding Climate Changes Utilizing GSSHA Model on the Bukhan River Basin. Master’s Thesis, Daejin University, Pocheon, Republic of Korea, 2022.
18. Ministry of Land, Infrastructure and Transport. *Soyangang River Basin Basic Plan (Amended) Report*; Ministry of Land, Infrastructure and Transport: Sejong, Republic of Korea, 2016.
19. Ministry of Land, Transport and Maritime Affairs. *North Han River Basin Basic Plan (Amended) Report*; Ministry of Land, Transport and Maritime Affairs: Sejong, Republic of Korea, 2012.
20. Ministry of Environment. *Guidelines for the Preparation of Land Cover Maps*; Ministry of Environment: Sejong, Republic of Korea, 2018.
21. Heo, K.S.; Jung, J.W. Hydrological Classification and Its Application of Korean Soil. *J. Korean Soc. Agric. Eng.* **1987**, *4*, 48–61.
22. Downer, C.W.; Ogden, F.L. *Gridded Surface Hydrologic Analysis (GSSHA) User’s Manual*; U.S. Army Corps of Engineers: Washington, DC, USA, 2006.
23. Pierre, Y.J.; Bahram, S.; Ogden, F.L. Raster-Based Hydrologic Modeling of Spatially-Variied Surface Runoff. *Am. Water Resour. Assoc.* **1995**, *31*, 523–535. [[CrossRef](#)]
24. Huggins, L.F.; Monke, E.J. *The Mathematical Simulation of the Hydrology of Small Watersheds*; Indiana Water Resources Research Center (IWRRC), Purdue University: Lafayette, Louisiana, 1966.
25. Engman, E.T. Roughness coefficients for routing surface runoff. *J. Irrig. Drain. Eng.* **1986**, *112*, 39–53. [[CrossRef](#)]
26. Park, S.S.; Lee, J.T. Determination of Surface Roughness Consider the Landuse and Classification Method. In Proceedings of the 34th Annual Conference and 2008 Civil Exposition, KSCE, Daejeon, Republic of Korea, 29 October 2008; pp. 564–567.
27. Hjelmfelt, A.T. Estimating Peak Runoff from Field-Size Watersheds. *JAWRA J. Am. Water Resour. Assoc.* **1986**, *22*, 267–274. [[CrossRef](#)]
28. Rawls, W.J. Estimating soil bulk density from particle size analysis and organic matter content. *Soil Sci.* **1983**, *135*, 123–125. [[CrossRef](#)]
29. Triadis, D.; Broadbridge, P. The Green-Ampt limit with reference to infiltration coefficients. *Water Resour. Res.* **2012**, *48*, 1–11. [[CrossRef](#)]
30. Ogden, F.L.; Sharif, H.O.; Senarath, S.U.S.; Smith, J.A.; Baeck, M.L.; Richardson, J.R. Hydrologic analysis of the Fort Collins, Colorado, flash flood of 1997. *J. Hydrol.* **2000**, *228*, 82–100. [[CrossRef](#)]
31. Ministry of Land, Infrastructure and Transport. *Inbukcheon River Basin Basic Plan (Amended) Report*; Ministry of Land, Infrastructure and Transport: Sejong, Republic of Korea, 2020.
32. Ministry of Land, Infrastructure and Transport. *Soyangang Upper River Basin Basic Plan (Amended) Report*; Ministry of Land, Infrastructure and Transport: Sejong, Republic of Korea, 2020.
33. Ogden, F.L.; Saghafian, B. Green and Ampt infiltration with redistribution. *J. Irrig. Drain. Eng.* **1997**, *123*, 386–393. [[CrossRef](#)]
34. Downer, C.W.; Ogden, F.L.; Martin, W.; Harmon, R.S. Theory, development, and applicability of the surface water hydrologic model CASC2D. *Hydrol. Process.* **2002**, *16*, 255–275. [[CrossRef](#)]
35. McDonald, M.G.; Harbaugh, A.W. *A Modular Three-Dimensional Finite-Difference Groundwater Flow Model*; U.S. Geological Survey Publication: Charleston, SC, USA, 1988.
36. Brevniva, E.V. Green-Ampt Infiltration Model Parameter Determination Using SCS Curve Number (CN) and Soil Texture Class, and Application to the SCS Runoff Model. Master’s Thesis, West Virginia University, Morgantown, WV, USA, 2001. [[CrossRef](#)]
37. Lee, J.; Jung, C.; Kim, S.; Kim, S. Assessment of Climate Change Impact on Future Groundwater Level Behavior Using SWAT Groundwater Consumption Function in Geum River Basin of South Korea. *Water* **2019**, *11*, 949. [[CrossRef](#)]

38. Ministry of Land, Transport and Maritime Affairs. *Groundwater Basic Survey Report for Chuncheon Area*; Ministry of Land, Transport and Maritime Affairs: Sejong, Republic of Korea, 2010.
39. National Groundwater Information Center. Groundwater Annual Report. 2022~2024. Available online: <https://www.gims.go.kr/internalAmount.do> (accessed on 11 September 2024).
40. Lee, J.M.; Go, K.S.; Nam, C.W. Characterization of Groundwater Level and Water Quality by Classification of Aquifer Types in South Korea. *Econ. Environ. Geol.* **2022**, *53*, 619–629. [[CrossRef](#)]
41. Nash, J.E.; Sutcliffe, J.V. River Flow Forecasting through Conceptual Model, Part 1-A Discussion of Principles. *J. Hydrol.* **1970**, *10*, 282–290. [[CrossRef](#)]
42. Boyle, D.P.; Gupta, H.V.; Sorooshian, S. Toward Improved Calibration of Hydrologic Models: Combining the Strengths of Manual and Automatic Methods. *J. Water Resour. Res.* **2000**, *36*, 3663–3674. [[CrossRef](#)]
43. Madsen, H. Automatic Calibration of a Conceptual Rainfall-runoff Model Using Multiple Objectives. *J. Hydrol.* **2000**, *235*, 276–288. [[CrossRef](#)]
44. Hong, W.Y.; Park, G.A.; Jung, I.K.; Kim, S.J. Development and Applicability Review of a Distributed Watershed Daily Runoff Model. *J. Korean Soc. Civ. Eng.* **2010**, *30*, 459–469.
45. Moriasi, D.N.; Gitau, M.W.; Pai, N.; Daggupati, P. Hydrologic and Water Quality Models: Performance Measures and Evaluation Criteria. *Am. Soc. Agric. Biol. Eng.* **2015**, *58*, 1763–1785. [[CrossRef](#)]
46. Willmott, C.J. On the Validation of Models. *Phys. Geogr.* **1981**, *2*, 184–197. [[CrossRef](#)]
47. Duda, P.B.; Hummel, P.R.; Donigian, A.S., Jr.; Imhoff, J.C. BASINS/HSPF: Model Use, Calibration, and Validation. *J. Am. Soc. Agric. Biol. Eng.* **2012**, *55*, 1523–1547. [[CrossRef](#)]
48. Chung, I.M.; Kim, N.W.; Lee, J.W. Estimation of Groundwater Recharge by Considering Runoff Process and Groundwater Level Variation in Watershed. *J. Soil Groundw. Environ.* **2007**, *12*, 19–32.

Disclaimer/Publisher’s Note: The statements, opinions and data contained in all publications are solely those of the individual author(s) and contributor(s) and not of MDPI and/or the editor(s). MDPI and/or the editor(s) disclaim responsibility for any injury to people or property resulting from any ideas, methods, instructions or products referred to in the content.